A Hybrid Numerical Technique for Analysis and Design of Microwave Integrated Circuits

by
Ming Yu

B.S., Tsinghua University, 1985
M.S., Tsinghua University, 1986

A Dissertation Submitted in Partial Fulfillment of the
Requirements for the Degree of

DOCTOR OF PHILOSOPHY

in the Department of
Electrical and Computer Engineering Department

We accept this Dissertation as conforming
to the required standard

Dr. R. Vahldieck, Supervisor

Dr. J. Bornemann, Departmental Member

Dr. W. Hoefer, Departmental Member

Dr. C. Bradley, Outside Member

Dr. V. K. Tripathi, External Examiner (Oregon State Univ.)

Supervisor: Dr. R. Vahldieck

ABSTRACT

Miniature Hybrid Microwave Integrated Circuits (MHMIC's) in conjunction with Monolithic MIC's (MMIC's) play an important role in modern telecommunication systems. Accurate, fast and reliable analysis tools are crucial to the design of MMIC's and MHMIC's. The space-spectral domain approach (SSDA) is such a numerically efficient method, which combines the advantage of the one-dimensional method of lines (MoL) with that of the one-dimensional spectral-domain method (SDM). In this dissertation, the basic idea of the SSDA is first introduced systematically. Then, a quasi-static deterministic variation of the SSDA is developed to analyze and design low dispersive 3-D MMIC's and MHMIC's. S-parameters and equivalent circuit elements for discontinuities are investigated. This includes air bridges, smooth transitions, open ends, step in width and gaps in coplanar waveguide (CPW) or microstrip type circuits. Experimental work is done to verify the simulation.

The full-wave SSDA is a more generalized and field theoretically exact numerical tool to model also dispersive circuits. The new concept of self-consistent hybrid boundary conditions to replace the modal source concept in the feed line is used here. In parallel, a deterministic approach is developed. Scattering parameters for some multilayered planar discontinuities including dispersion effect are calculated to validate this method.

Examiners

Dr. R. Vahldieck, Supervisor

Dr. J. Bornemann, Departmental Member

Dr. W. Hoefer, Departmental Member

Dr. C. Bradley, Outside Member

Dr. V. K. Tripathi, External Examiner (Oregon State Univ.)

Table of Contents

List of Figures

List of Tables

Acknowledgments

The author wishes to express his acknowledgments to his thesis supervisor, Dr. Ruediger Vahldieck, for his guidance, encouragement and invaluable suggestions throughout the course of this thesis.

Financial support for this research by Dr. R. Vahldieck (through NSERC), Science Council of British Columbia (through GREAT Award) and MPR Teltech Ltd. is also gratefully acknowledged. In particular, I would like to thank Dr. J. Fikart and H. Minkus, MPR Teltech, for the fabrication of the MHMIC prototypes. which were used to verify the SSDA results.

The author also wishes to extend his thanks to Dr. K. Wu for his invaluable suggestions. The author is also grateful to his colleagues at the Laboratory for Lightwave Electronics, Microwave and Communications (LLiMiC), University of Victoria for their support and discussion.

Last, but by no means least, the author wishes to express his thanks to his family, especially to his wife, Mei Li, for their support and encouragement.

Chapter 1

Introduction

1.1 Background and Goals

Miniaturization of microwave circuits is essential in the evolution of modern communications systems. In analogy to the miniaturization that has taken place in VLSI (Very Large Scale Integrated Circuits), Monolithic Microwave Integrated Circuits (MMIC's) but also Miniature Hybrid Microwave Integrated Circuits (MHMIC's) combine a steadily growing number of microwave components on smaller and smaller chip real estate. MMIC's as shown in Figure 1.1 [14] are very expensive in the fabrication and are only justified for large volume applications. MHMIC's are a hybrid technology that is in particular suitable for small to medium volume applications. While MMIC's require semiconductor fabrication facilities (circuits are grown on CaAs), which are capable to integrate active devices like FET's (Field Effect Transistors) in one process on the same wafer, MHMIC's are grown on alumina substrate as shown in Figure 1.2, and active devices are wire bonded into the chip in a final fabrication step. The latter technology is less attractive for large volume applications because of the additional labor involves, but offers better circuit performance and is less expensive for small to medium applications. Both MMIC's and MHMIC's play an important role in modern communication systems.

A serious bottleneck in both technologies is the lack of accurate, fast and reliable design strategies. Although commercial design software is available, the numerical methods used are either computationally very inefficient or inaccurate at higher frequencies. Several fabrication cycles become necessary to trim the circuit so that it satisfies the design requirements. This process is very expensive and time-consuming (several months). To cut down on the processing time and cost, it is necessary to develop accurate design algorithms for MMIC's and MHMIC's in order to achieve first-pass success.

In general, numerical methods can be classified into two categories:

1. Methods which use an eigenmode approach to describe the electromagnetic field

e.g.,

- ***Mode Matching Method*** *(MMM) [1]*
- ***Spectral Domain Method*** *(SDM) [2 - 5]*

2. *Methods which discretize a differential operator*

e.g.,

- ***Finite Difference Method*** *(FDM) [6]*
- ***Method of Lines (MOL)*** *[7]-[13]*

The first category of methods use orthogonal modes or basis functions to expand the field directly.

The second category of methods is applied directly to either Maxwell's or the Helmholtz equations. The first and second differential operator are approximated by finite differences.

Both category of methods can be subdivided further into

Quasi-static techniques *which calculate equivalent network parameters. Microwave circuits are described by lumped elements like capacitors and inductors, which are assumed to be constant over frequency.*

Full-wave techniques *which describe the electromagnetic field directly from Maxwell's equations. Circuits are considered from the field theory point of view and may be described by S-parameters, which include*

the interaction of fundamental and higher order modes at discontinuities.

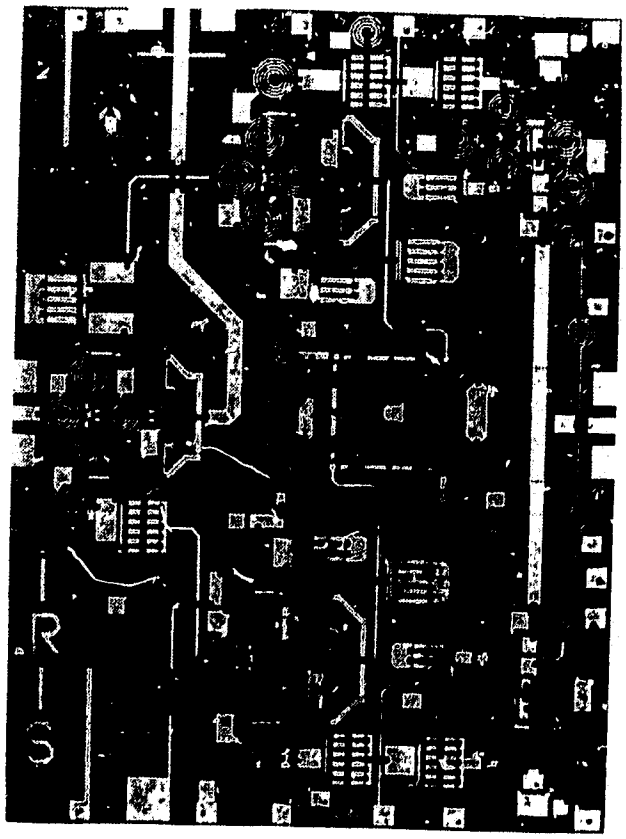

Figure 1.1 Example for an MMIC Circuit

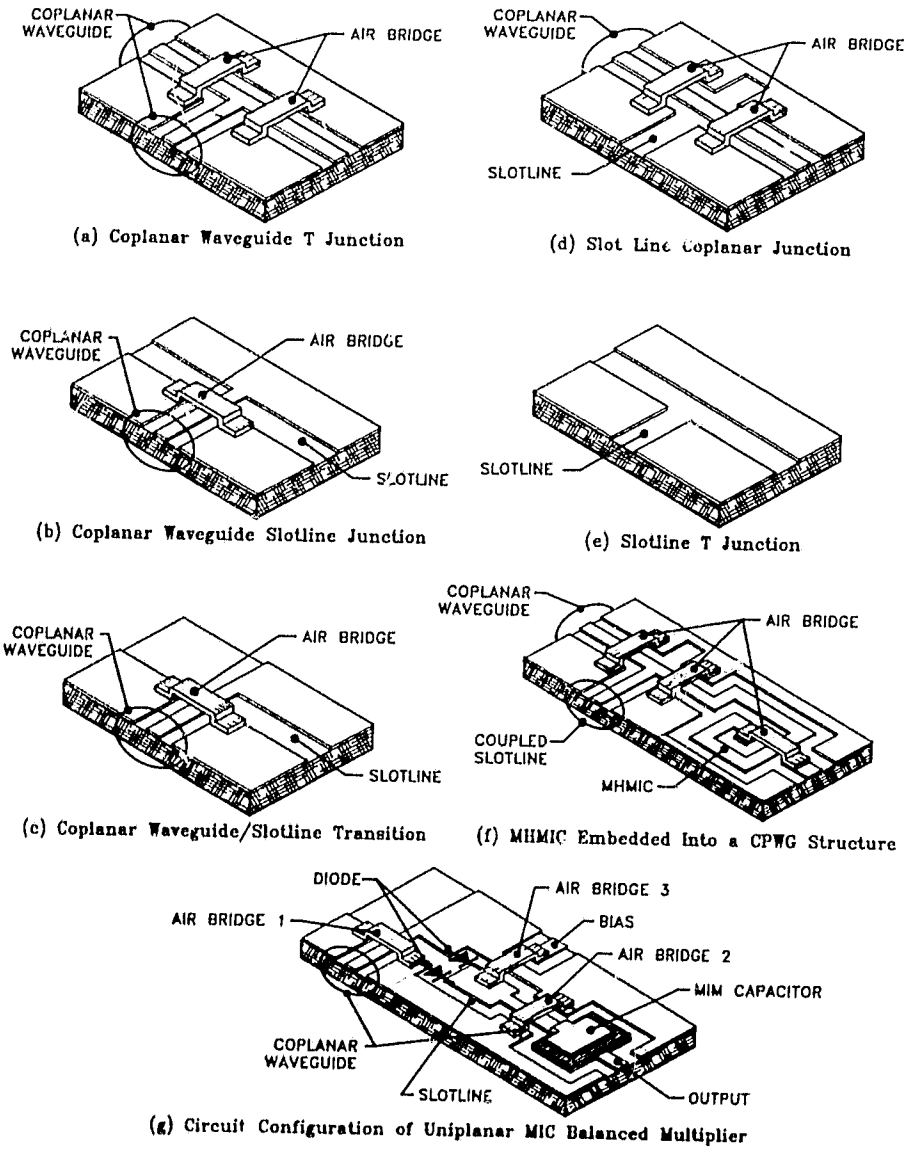

Figure 1.2 MHMIC discontinuities

Quasi-static numerical techniques are traditionally faster than full-wave techniques, in particular, on the serial machines widely used today. These methods do not benefit from the availability of parallel processors. For some applications, their accuracy can rival that of full wave techniques and, therefore, they are very useful engineering design tools.

Theoretically speaking, a quasi-static approach only works at zero frequency. However, as long as the dimensions of circuits are small compared with the wavelength and the dispersion of the transmission line system is weak or non-existing, quasi-static methods can work up to the millimeter-wave range. A large number of commercially available software is built on quasi-static methods. In most cases the equivalent element values derived from quasi-static methods are assumed to be constant over the frequency. Furthermore, it is assumed that the discontinuities for which they are derived do not radiate or interfere with each other. This assumption becomes invalid the closer microwave elements are placed on the chip. In this case the predicted performance of the MMIC's or MHMIC's may deviate significantly from the required performance.

For structures, or frequencies, at which quasi-static methods do not provide accurate results, either because the circuit density is too high or dispersion effects are too significant, full-wave modelling of microwave and millimeter-wave circuits becomes necessary. In this dissertation, a generalized Space-Spectral Domain Approach is first introduced that is suitable for this task. Secondly, a new quasi-static deterministic technique will be presented. Finally, two SSDA full-wave algorithms will be discussed.

Typical generalized full-wave approaches are, e.g., the Finite Difference Method (FDM) or Transmission Line Matrix (TLM) [16] method. These methods start directly from Maxwell's equations with very little approximation and virtually no analytical preprocessing. They have almost no structural limitations and provide a high degree of accuracy. Being very flexible, they often require large amounts of computer memory and long computer run-time, at least on most of today's available engineering workstations. To speed these methods up, parallel processor machines are required which, for some time to come, will not be commonly used in engineering laboratories because of the special program languages necessary to fully take advantage of the potential of these machines.

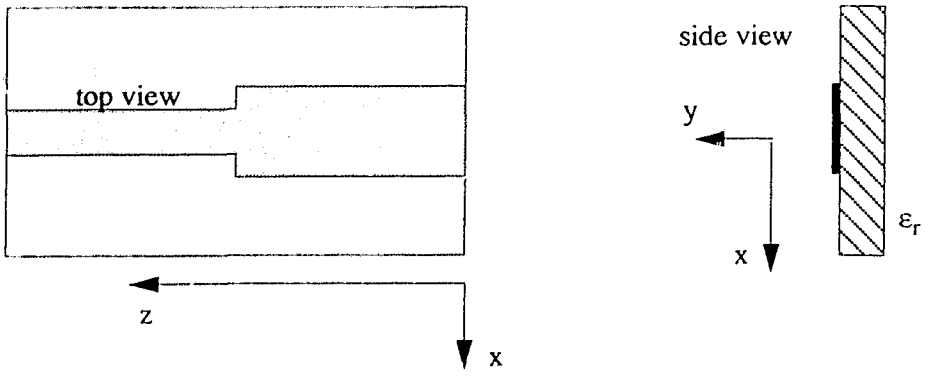

Figure 1.3 A typical planar discontinuity

When dealing with the analysis and design of MMIC's and MHMIC's, their quasi-planar structure, as shown in Figure 1.3, allows the use of less generalized but computationally more efficient techniques. In the past, the most suitable methods for 3-D planar circuit analysis have been the Spectral Domain Method (SDM), the Mode Matching Method (MMM), and the Method of Lines (MoL) (full-wave and quasi-static).

In the SDM, the Fourier transform is taken along a direction parallel to the substrate, and Galerkin's technique is used to yield a homogeneous system of equations. To determine the eigenvalue problem (propagation constant) in a planar circuit, the 1-D SDM is well known for its fast computational algorithm and minimum memory requirements. But the SDM also requires that the circuit discontinuities fit into an orthogonal coordinate system and, especially, that the basis functions are chosen carefully. For 3-D discontinuity analysis, the 2-D SDM requires usually a large number of two-dimensional basis functions which are not easy to chose and handle and which increase the computation time significantly because of potential convergence problems [43].

The MoL is a space-frequency domain method similar to the FDM but uses an orthogonal transform. To treat 3-D discontinuities, the 2-D MoL is used, which discretizes the two spatial variables parallel to the substrate plane while an analytical solution is obtained in the direction perpendicular to the substrate plane. This method requires only a two-dimensional discretization for a general 3-D problem. The advantage of this method is its easy formulation, simple convergence behavior and the fact that there are no special basis functions necessary. The disadvantages of the 2-D MoL is that satis-

fying all boundary conditions simultaneously for arbitrarily shaped circuits may be very difficult or may require a very fine 2-D discretization. In short, when applying the SDM or MoL to an arbitrary 3-D discontinuity problem, each method by itself encounters a number of serious problems which are inherent in the method.

To overcome the inherent limitation of each method, a new hybrid numerical method has been developed by Wu and Vahldieck [17]. This method is called the Space-Spectral Domain Approach (SSDA) which combines the 1-D SDM and 1-D MoL. This new method eliminates the shortcomings of the conventional 2-D MoL and 2-D SDM and takes advantage of the attractive features associated with the 1-D SDM and the 1-D MoL. The SSDA is developed in particular for the analysis of arbitrarily shaped spatial 3-D planar discontinuities.

In this dissertation, we first introduce the generalized SSDA concept which is extended from the work of Wu and Vahldieck [17]. Although this analysis can only be applied to calculate resonant frequencies but not discontinuity S-parameters, it is used to explain the basic idea of the SSDA. On that basis, a new deterministic quasi-static SSDA [18], [20] is presented followed by a full-wave SSDA [19], which is aimed at the calculation of S-parameters in structures supporting hybrid modes.

1.2 Organization of This Dissertation

Chapter 2 reviews the SDA and MoL and investigates their relationship, which forms the basis of the SSDA. The generalized SSDA is introduced in a planar resonator problem which forms the basis of this dissertation.

Chapter 3 introduces the quasi-static SSDA.

Chapter 4 introduces the full-wave SSDA.

Chapter 5 discusses simulation results and their experimental verification.

Chapter 6 concludes the dissertation.

Chapter 2

The Space-Spectral Domain Approach

In this chapter, the Spectral Domain Method (SDM), the Method of Lines (MoL) as well as the relationship between both methods are first reviewed. The concept of the Space-Spectral Domain Approach (SSDA) is introduced as a combination of the SDM and the MoL. For a three-dimensional (3-D) electromagnetic problem, the SDM is applied to the x-direction, the MoL is applied to the z-direction, and the analytical process is applied to the y-direction (see Figure 2.1).

2.1 The Spectral Domain Method

Figure 2.1 is a 3-D version of Figure 1.3; it shows a typical planar circuit discontinuity in a shielded box. In the Spectral Domain Method the Fourier transform is taken along the x-direction for a 2-D problem and always along the x- and z-direction for a 3-D problem. The analysis in the Fourier transform domain was first introduced by Yamashita and Mittra [2] for computation of the characteristic impedance and the phase velocity of a microstrip line based on a quasi-static approach. It is one of the most popular and widely used numerical techniques for planar circuits. Numerous publications can be found in the literature, e.g., [3 - 5].

For planar transmission line and discontinuity problems, the electric and magnetic fields E and H are often written in terms of scalar potentials Ψ^e and Ψ^h in a Cartesian coordinate system, shown in Figure 2.1 (this is called a TE_z / TM_z formulation)

$$\begin{aligned} E &= -\nabla\times\left(\Psi^h\hat{z}\right) + \frac{1}{j\omega\varepsilon}\nabla\times\nabla\times\left(\Psi^e\hat{z}\right) \\ H &= \nabla\times\left(\Psi^e\hat{z}\right) + \frac{1}{j\omega\mu}\nabla\times\nabla\times\left(\Psi^h\hat{z}\right) \end{aligned} \tag{2.1}$$

where $\hat{z}$ is the unit vector in z-direction. $\Psi^{e,h}$ satisfy the wave equation

$$\frac{\partial^2 \Psi^{e,h}}{\partial x^2} + \frac{\partial^2 \Psi^{e,h}}{\partial y^2} + \frac{\partial^2 \Psi^{e,h}}{\partial z^2} + k^2 \Psi^{e,h} = 0 \qquad (2.2)$$

$$k^2 = \omega^2 \mu \varepsilon$$

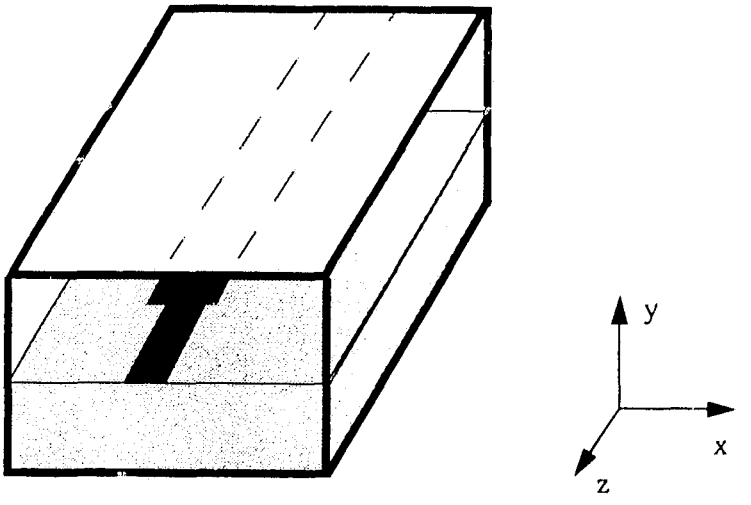

Figure 2.1 A shielded microstrip line

The idea of the SDM is to apply the Fourier transform along the x-direction in order to eliminate the space variable x and replace it with a spectral term α_x

$$\psi^{e,h} = \int_{-\infty}^{\infty} \Psi^{e,h} e^{j\alpha x} dx \qquad (2.3)$$

Assuming the problem is a two-dimensional one in x- and y-direction, with the propagation constant β in z-direction, equation (2.2) yields

$$-\alpha^2 \psi^{e,h} + \frac{\partial^2 \psi^{e,h}}{\partial y^2} - \beta^2 \psi^{e,h} + k^2 \psi^{e,h} = 0 \qquad (2.4)$$

The above equation (2.4) can be further simplified as a one-dimensional normal dif-

ferential equation

$$\frac{\partial^2 \psi^{e,h}}{\partial y^2} - \left(\alpha^2 + \beta^2 - k^2\right)\psi^{e,h} = 0 \tag{2.5}$$

By applying the boundary conditions (more details will be given in Section 2.4), one finally obtains an algebraic equation in matrix form

$$\begin{bmatrix} e_x \\ e_z \end{bmatrix} = [Z] \begin{bmatrix} j_x \\ j_z \end{bmatrix} \tag{2.6}$$

e_x and e_z are the Fourier transforms of the electrical field in the x- and z-direction. j_x and j_z are the Fourier transforms of the current in the x- and z-direction. The unknown j_x and j_z are expanded in terms of known basis functions with unknown weighting coefficients. By applying Galerkin's technique, the propagation constant and field distribution can be found.

In summary, the SDM has several features:

- Simple formulation in the form of algebraic equations
- Utilization of a-priori (physical) knowledge of modes
- Numerically efficient

The SDM is well known for its computational efficiency and minimum memory requirement for two-dimensional problems (1-D SDM) because usually only a few basis functions are needed. The SDM loses some of its advantages when applied to spatial three-dimensional discontinuities (2-D SDM). In particular when these discontinuities are arbitrarily shaped, it becomes generally a problem to find suitable basis functions and to achieve reasonable convergence.

2.2 The Method of Lines

The Method of Lines (MoL) was first developed by mathematicians [7] in order to solve differential equations. It was applied to microwave analysis and design problems by Pregla and co-authors [8 - 13].

The concept of the MoL is as follows: for a given system of partial differential

equations, all but one of the independent variables are discretized to obtain a system of ordinary differential equations so that the whole space is represented by a number of lines. This semi-analytical procedure is very useful in the calculation of planar transmission line structures.

To demonstrate the basic steps of the MoL, consider the microstrip line cross-section in Figure 2.2

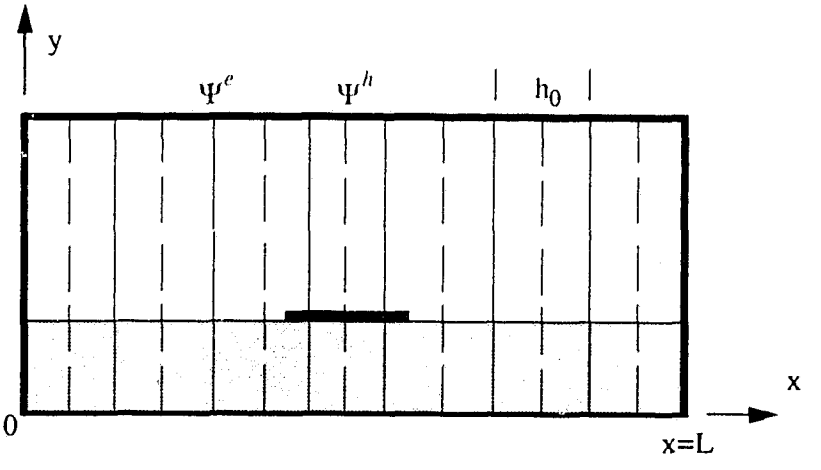

Figure 2.2 Cross-section view of a microstrip line

Equation (2.2) is to be solved here. The discretization is done in the x-direction as shown above. The figure also shows that two separate line systems are used to represent Ψ^e and Ψ^h. This shifting scheme has several advantages: the lateral boundary conditions are easily fulfilled, it allows an optimal edge condition [10], second order accuracy [11] and simple matrix formulation.

Let the number of Ψ^e and Ψ^h lines in Figure 2.2 be equal to N_z. The potentials on all the lines are combined to form a vector $\vec{\Psi}^e$ and $\vec{\Psi}^h$, respectively. Equation (2.2) can then be rewritten as

$$\frac{\partial^2 \vec{\Psi}^{e,h}}{\partial x^2} + \frac{\partial^2 \vec{\Psi}^{e,h}}{\partial y^2} + \frac{\partial^2 \vec{\Psi}^{e,h}}{\partial z^2} + k^2 \vec{\Psi}^{e,h} = 0 \tag{2.7}$$

The first derivative with respect to x is formed as backward difference quotients for Ψ^e and forward difference quotients for Ψ^h

$$h_0 \frac{\partial \hat{\Psi}^e}{\partial x} \rightarrow [D]\hat{\Psi}^e$$
$$h_0 \frac{\partial \hat{\Psi}^h}{\partial x} \rightarrow -[D]^t \hat{\Psi}^h \tag{2.8}$$

with

$$[D] = \begin{bmatrix} 1 & \dots & 0 & 0 \\ -1 & \dots & 0 & \dots \\ \dots & \dots & \dots & 1 \\ 0 & \dots & 0 & -1 \end{bmatrix} \tag{2.9}$$

In the difference operator $[D]$ the lateral boundary conditions are included (here a Dirichlet-Neumann boundary condition is used as an example). The second derivatives can also be represented by means of the operator $[D]$

$$h_0^2 \frac{\partial^2 \hat{\Psi}^e}{\partial x^2} \rightarrow -\left[D_{xx}^e\right]\hat{\Psi}^e$$
$$h_0^2 \frac{\partial^2 \hat{\Psi}^h}{\partial x^2} \rightarrow -\left[D_{xx}^h\right]\hat{\Psi}^h \tag{2.10}$$

Equation (2.7) can then be written as

$$\frac{\partial^2 \hat{\phi}^{e,h}}{\partial y^2} - \left(\delta_{e,h}^2 + \beta^2 - k^2\right)\hat{\phi}^e = 0 \tag{2.11}$$

where

$$\hat{\phi}^{e,h} = \left[T^{e,h}\right]^{-1} \hat{\Psi}^{e,h} \tag{2.12}$$

$$\frac{1}{h_0^2}\left[T^{e,h}\right]^t\left[D_{xx}^{e,h}\right]\left[T^{e,h}\right] = \delta_{e,h}^2$$

$$\left[D_{xx}^{e}\right] = -[D]^t[D] \qquad \left[D_{xx}^{h}\right] = -[D][D]^t \tag{2.13}$$

$\delta_{e,h}^2$ is the eigenvalue matrix and $\left[T^{e,h}\right]$ the eigenvector belonging to $\left[D_{xx}^{e,h}\right]$ which can be obtained analytically dependent on the different lateral boundary conditions [11]. For example, for the structure shown in Figure 2.2, the elements of $\left[T^{e}\right]$ are

$$T_{i,n}^{e} = \sin\frac{in\pi}{N+1} \qquad i, n = 1, \ldots, N \tag{2.14}$$

Equation (2.12) is called the orthogonal transform because $\left[D_{xx}^{e,h}\right]$ is a symmetrical matrix and $\left[T^{e,h}\right]$ is an orthogonal matrix. Equation (2.11) is in the transform domain, which is similar to equation (2.5) in the Fourier domain. However, the way to solve equation (2.5) and equation (2.11) are different in either techniques. By applying lateral boundary conditions, a system equation similar to equation (2.6) can be obtained. Applying the orthogonal transform a new algebraic system equation can be derived in the (original) spatial domain ([11] gives more details)

$$\begin{bmatrix}\hat{E}_x\\ \hat{E}_z\end{bmatrix} = [Z]\begin{bmatrix}\hat{J}_x\\ \hat{J}_z\end{bmatrix} \tag{2.15}$$

The vector notation is used here to represent discretized quantities. Because equation (2.15) is in the spatial domain, it can be simplified by removing those lines which do not pass through the metallization at the interface

$$0 = [Z_r]\begin{bmatrix}\hat{J}_{rx}\\ \hat{J}_{rz}\end{bmatrix} \tag{2.16}$$

The propagation constant and field distribution can be calculated by solving the root of the determinant of $[Z_r]$, where subscript r signifies that $[Z_r]$ is a residual matrix.

For three-dimensional problems also the z-varible is discretized (2-D MoL).

In summary, the 1-D MoL has the following features:

- No basis function needed
- Simple formulation and efficient calculation
- No relative convergence phenomenon

However, similar to the SDM, when applied to three-dimensional problems, the 2-D MoL becomes numerically less efficient because of the two-dimensional discretization.

2.3 The Relationship Eetween the SDM and MoL

From the previous sections, it is quite obvious that both methods, the SDM and MoL, have some similarities if one compares equations (2.3), (2.5) and equations (2.11), (2.12). The following analysis shows that the MoL is indeed related to the SDM and that this relationship helps to combine the advantages of both methods into one new method, the Space-Spectral Domain Approach.

This becomes obvious if one rewrites equation (2.2) for the two-dimensional transmission line problem (the superscripts of Ψ are removed without loss of generality)

$$\frac{\partial^2 \Psi}{\partial x^2} + \frac{\partial^2 \Psi}{\partial y^2} - \left(\beta^2 - k^2\right)\Psi = 0 \tag{2.17}$$

where β is the propagation constant.

In both the MoL and SDM, a transformation is performed in the x-direction

$$\begin{aligned} &MoL \qquad \Psi \Rightarrow \vec{\Psi} \qquad \vec{\Psi} \Rightarrow \vec{\phi} \qquad \vec{\phi} = [T]\vec{\Psi} \\ &SDM \qquad \Psi \Rightarrow \tilde{\psi} \qquad \tilde{\psi} = \int_{-\infty}^{\infty} \Psi e^{j\alpha x} dx \end{aligned} \tag{2.18}$$

which leads to a one-dimensional normal differential equation that corresponds to equation (2.5) and equation (2.11).

From equation (2.18) one may deduce that the orthogonal transform in the MoL represents a discrete Fourier transform in matrix form. Although in [11] some analysis is provided to support this point, there is no clear explanation to prove that the MoL

scheme (discretization and orthogonal transform) and the SDM are truly identical. Furthermore, also the connection between the SDM, the MoL and the SSDA has not been investigated in detail. The following analysis is intended to fill this gap.

To demonstrate the relationship between the SDM and the MoL, the structure in Figure 2.2 is used again. (Dirichlet boundary condition is applied for the electric potential Ψ^e at $x=0$ and at $x=L$) The Fourier expansion in region $[0, L]$ is written as

$$\psi^e = \int_0^L \Psi^e \sin \alpha x dx \qquad \alpha = \frac{i\pi}{L} \qquad i = -\infty, \ldots, \infty \tag{2.19}$$

If the potential is discretized into N points in the x-direction, i.e. $x \to x_n = \frac{n}{N_z + 1} L$, $i=1,\ldots, N_z$, and N_z spectral terms are used,

$$\psi_i^e = \sum_{n=1}^{N_z} \Psi_n^e \sin \frac{in\pi}{N_z + 1} \qquad i = 1, \ldots, N_z \tag{2.20}$$

The subscripts are used to represent discrete quantities and discrete spectral terms. If vectors are used to represent discretization, equation (2.20) can be rewritten as

$$\vec{\psi}^e = \left[\Gamma^e\right] \Psi^e \tag{2.21}$$

where the element of $\left[\Gamma^e\right]$

$$\Gamma_{i,n}^e = \sin \frac{in\pi}{N_z + 1} \tag{2.22}$$

From here one may compare

$$\begin{aligned} MoL \qquad & \dot{\vec{\phi}}^e = \left[T^e\right] \vec{\Phi}^e \\ SDA \qquad & \dot{\vec{\psi}}^e = \left[\Gamma^e\right] \vec{\Psi}^e \end{aligned} \tag{2.23}$$

From equation (2.14)

$$\left[\Gamma^e\right] = \left[T^e\right] \tag{2.24}$$

This shows that the MoL is a discrete SDM. The equivalence of the MoL and the SDM is established under the same finite discretization scheme. From another point of view, because the SDM (theoretically) uses an infinite number of spectral terms, the SDM gives an infinite number of precise eigenvalues and eigenfunctions which can be solved using analytical transforms while the MoL yields a finite number of approximate eigenvalues and eigenfunctions which can be solved using finite discretization.

In summary the following properties are found comparing the SDM and MoL

- The SDM and MoL are indeed related to each other.
- Both of them are numerically very efficient for 2-D problems and less efficient for 3-D problems.

Combining the MoL and SDM will take the advantage of both methods to analyze 3-D problems more efficiently. This leads to the invention of a new method called the Space-Spectral Domain Approach (SSDA).

2.4 The Space-Spectral Domain Approach

This section describes the basic principles of the Space-Spectral Domain Approach (SSDA). The SSDA was first introduced by Wu and Vahldieck [17] and further developed by the author together with Wu and Vahldieck [18 - 20]. First, a generalized introduction is given for a 3-D planar resonator circuit.

The two techniques combined in the SSDA are the SDM to simulate the cross section of transmission line structures and the MoL to model their longitudinal direction. The microstrip line step discontinuity shown in Figure 2.3 is taken as an example to demonstrate the basic steps involved. In this chapter only the homogenous boundary condition is considered (the discontinuity is enclosed in a shielding box).

First of all a combination of electric and magnetic lines are introduced to discretize the structure in the z-direction. This corresponds to slicing the structure in the x-y plane. Then a set of conventional basis functions for each slice is introduced which satisfy the boundary conditions along the x-coordinate. Every slice is of regular rectangular shape, so that only well known conventional 1-D basis functions are needed. The Fourier transform is performed to replace the x-coordinate in the Helmholtz equation with the spectral

term ω. Since the MoL procedure is used in z-direction, the resulting wave equations are coupled. The orthogonal transform in the spatial domain is utilized to decouple the system equations. The three spatial variables in the Helmholtz equation are now reduced to the remaining y variables and can therefore be solved analytically. The advantage of this procedure is that fine circuit details such as narrow strips and slots as well as complicated discontinuity shapes can be easily resolved by discretizing the structure in z-direction. Furthermore, problems such as complicated basis functions, huge memory space and long CPU time known from the 2-D SDM or MoL (i.e. 3-D problems) are avoided. The final steps of the SSDA are: the boundary conditions between layers at the top and bottom of the closed structure are transformed into the circuit plane. Satisfying the boundary conditions at that location leads to a set of equations which are the Green's functions by nature. After transforming these final equations into the spatial domain, Galerkin's technique is applied so that a characteristic matrix equation is obtained. By introducing hybrid boundary conditions, the S-parameters can be obtained. This will be discussed in Chapter 4.

2.4.1 SDM in x-direction

The cross-section of a microstrip resonator is shown in Figure 2.3. Although a single layer structure is drawn for the purpose of simplicity, the following formulations are also valid for a multilayer structure (y_k and y_m are used here for a generalized formulation). The electromagnetic field in the p^{th} layer can be expressed in terms of scalar potential functions according to equation (2.1)

$$\begin{aligned} E &= -\nabla\times\left(\Psi^{h}_{\hat{z}}\right) + \frac{1}{j\omega\varepsilon_0\varepsilon_r^p}\nabla\times\nabla\times\left(\Psi^{e}_{\hat{z}}\right) \\ H &= \nabla\times\left(\Psi^{e}_{\hat{z}}\right) + \frac{1}{j\omega\mu}\nabla\times\nabla\times\left(\Psi^{h}_{\hat{z}}\right) \end{aligned} \tag{2.25}$$

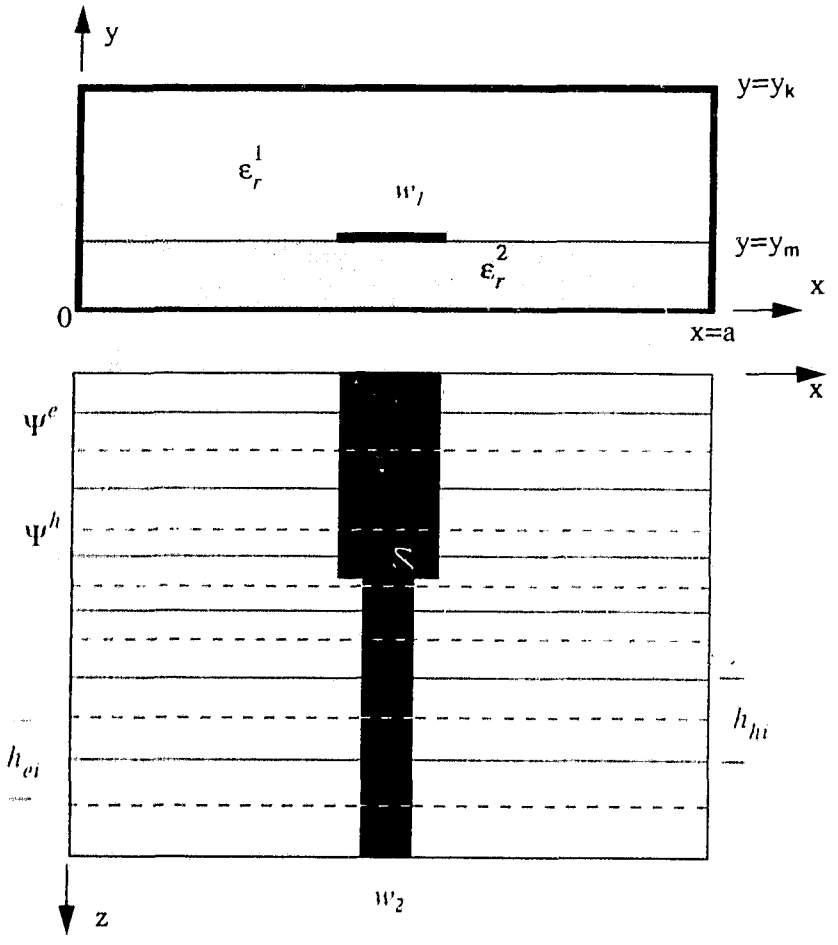

Figure 2.3 A microstrip discontinuity in a resonator enclosure

Ψ^e and Ψ^h are the solutions of the partial differential Helmholtz equation pair

$$\frac{\partial^2 \Psi^{e,h}}{\partial x^2} + \frac{\partial^2 \Psi^{e,h}}{\partial y^2} + \frac{\partial^2 \Psi^{e,h}}{\partial z^2} + \varepsilon_r^p k_0^2 \Psi^{e,h} = 0 \qquad (2.26)$$

$$k_0^2 = \omega^2 \mu \varepsilon_0$$

where

ε^p_r is the relative dielectric constant in the p^{th} layer. The Fourier transform is

applied in x-direction

$$\Psi^{e,h} \rightarrow \psi^{e,h} \tag{2.27}$$

$$\psi^{e,h} = \int_{-\infty}^{\infty} \Psi^{e,h} e^{j\alpha x} dx \tag{2.28}$$

where α is the space-spectral variable.

The electric and magnetic field vectors in equation (2.25) will take the following form in the spectral domain

$$\tilde{e} = \int_{-\infty}^{\infty} E e^{j\alpha x} dx \qquad \tilde{h} = \int_{-\infty}^{\infty} E e^{j\alpha x} dx \tag{2.29}$$

The space-spectral domain Helmholtz equation can now be written as:

$$\frac{\partial^2 \psi^{e,h}}{\partial y^2} + \frac{\partial^2 \psi^{e,h}}{\partial z^2} - \left(\alpha^2 - \varepsilon_r^p k_0^2\right) \psi^{e,h} = 0 \tag{2.30}$$

2.4.2 MoL in z-direction

After the Fourier transform has been applied in x-direction, the Method of Lines (MoL) can be applied in z-direction. The structure is sliced in the x-y plane at each z-coordinate. The electric lines and magnetic lines are introduced to represent the discretized scalar potentials in the spatial Fourier transform domain. A total number of N_z lines are used for different types of transmission line configuration.

In vector notation the discretized potentials $\psi^{e,h}$ are written as a N_z-element vector as described in Section 2.2 .

$$\psi^{e,h} \rightarrow \vec{\psi}^{e,h} \tag{2.31}$$

Non-equidistant discretization [15] can be used here to increase the flexibility. The non-equidistant discretization can also be considered as a linear transform from $\vec{\psi}^{e,h}$ (original vector) to $\vec{\Phi}^{e,h}$ (non-equidistant discretized vector)

$$\vec{\psi}^{e,h} \rightarrow \vec{\varphi}^{e,h} \tag{2.32}$$

The new potential $\vec{\varphi}^{e,h}$ is defined as

$$\vec{\varphi}^{e,h} = \left[r_{e,h}\right]^{-1} \vec{\psi}^{e,h} \tag{2.33}$$

where

$$\left[r_{e,h}\right] = diag\left(\sqrt{\frac{h_0}{h_{e,hi}}}\right) \tag{2.34}$$

$h_{e,hi}$ denotes the discretization interval of electric and magnetic lines, respectively. h_0 is the limiting case for the discretization interval (equidistant discretization).

The finite difference expression of the first derivative is written in matrix notation

$$\begin{aligned} h_0 \frac{\partial \vec{\varphi}^{e}}{\partial z} &\rightarrow \left[D_z\right] \vec{\varphi}^{e} \\ h_0 \frac{\partial \vec{\varphi}^{h}}{\partial z} &\rightarrow -\left[D_z\right]^t \vec{\varphi}^{h} \end{aligned} \tag{2.35}$$

where

$$\left[D_z\right] = \frac{1}{h_0}\left[r_h\right]\left[D\right]\left[r_e\right] \tag{2.36}$$

$[D]$ is defined in equation (2.9). The second order derivatives can be written as

$$\begin{aligned} h_0^2 \frac{\partial^2 \vec{\varphi}^{e}}{\partial z^2} &\rightarrow -\left[D^e_{zz}\right] \vec{\varphi}^{e} \\ h_0^2 \frac{\partial^2 \vec{\varphi}^{h}}{\partial z^2} &\rightarrow -\left[D^h_{zz}\right] \vec{\varphi}^{h} \end{aligned} \tag{2.37}$$

where

$$\left[D^e_{zz}\right] = -\left[D_z\right]^t\left[D_z\right] \qquad \left[D^h_{zz}\right] = -\left[D_z\right]\left[D_z\right]^t \tag{2.38}$$

Because $[D^{e,h}{}_{zz}]$ is a symmetrical matrix, the following transforms can be applied

to transform this matrix into a diagonal form:

$$\frac{1}{h_0^2}\left[T^e\right]^t\left[D_{zz}^e\right]\left[T^e\right] = \delta_{ee}^2 \qquad \frac{1}{h_0^2}\left[T^h\right]^t\left[D_{zz}^h\right]\left[T^h\right] = \delta_{hh}^2 \tag{2.39}$$

Similar to Section 2.2 , a new potential in the (orthogonal) transform domain is defined as

$$\hat{V}^{e,h} = \left[T^{e,h}\right]^{-1}\hat{\Phi}^{e,h} \tag{2.40}$$

The final 1-D Helmholtz equations in the transformation domain are derived from equation (2.30)

$$\begin{aligned}\frac{\partial^2 \hat{V}^e}{\partial y^2} - \left(\delta_{ee}^2 + \alpha^2 - \varepsilon_r^p k_0^2\right)\hat{V}^e &= 0 \\ \frac{\partial^2 \hat{V}^h}{\partial y^2} - \left(\delta_{hh}^2 + \alpha^2 - \varepsilon_r^p k_0^2\right)\hat{V}^h &= 0\end{aligned} \tag{2.41}$$

The analytical solutions of the above N_z decoupled equations can be expressed as transmission line equations from point y_m to y_k. The i^{th}component is

$$\begin{bmatrix} V_i^e \\ \dfrac{\partial V_i^e}{\partial y}\end{bmatrix}_{y_k} = \begin{bmatrix} \cosh\gamma_{ei}d_i & \dfrac{1}{\gamma_{ei}}\sinh\gamma_{ei}d_i \\ \gamma_{ei}\sinh\gamma_{ei}d_i & \cosh\gamma_{ei}d_i \end{bmatrix}\begin{bmatrix} V_i^e \\ \dfrac{\partial V_i^e}{\partial y}\end{bmatrix}_{y_m} \tag{2.42}$$

$$\begin{bmatrix} V_i^h \\ \dfrac{\partial V_i^h}{\partial y}\end{bmatrix}_{y_k} = \begin{bmatrix} \cosh\gamma_{hi}d_i & \dfrac{1}{\gamma_{hi}}\sinh\gamma_{hi}d_i \\ \gamma_{hi}\sinh\gamma_{hi}d_i & \cosh\gamma_{hi}d_i \end{bmatrix}\begin{bmatrix} V_i^h \\ \dfrac{\partial V_i^h}{\partial y}\end{bmatrix}_{y_m} \tag{2.43}$$

where

$$\begin{aligned}\gamma_{ee}^2 &= \delta_{ee}^2 + \alpha^2 - \varepsilon_r^p k_0^2 \\ \gamma_{hh}^2 &= \delta_{hh}^2 + \alpha^2 - \varepsilon_r^p k_0^2\end{aligned} \qquad d_i = y_k - y_m \tag{2.44}$$

The equation (2.42) and (2.43) can also be represented in matrix form as:

$$\begin{bmatrix} \hat{V}^e \\ \frac{\partial \hat{V}^h}{\partial y} \\ \frac{\partial \hat{V}^e}{\partial y} \\ \hat{V}^h \end{bmatrix}_{y_k} = [Q_p] \begin{bmatrix} \hat{V}^e \\ \frac{\partial \hat{V}^h}{\partial y} \\ \frac{\partial \hat{V}^e}{\partial y} \\ \hat{V}^h \end{bmatrix}_{y_m} \tag{2.45}$$

where $[Q_p]$ is a $4N_z$ by $4N_z$ matrix

$$[Q_p] = \begin{bmatrix} [C_e] & [0] & [S_{e1}] & [0] \\ [0] & [C_h] & [0] & [S_{h2}] \\ [S_{e2}] & [0] & [C_e] & [0] \\ [0] & [S_{h1}] & [0] & [C_h] \end{bmatrix} \tag{2.46}$$

$$\begin{aligned} [C_e] &= diag(\cosh\gamma_{ei}d_i) & [C_h] &= diag(\cosh\gamma_{hi}d_i) \\ [S_{e1}] &= diag(\sinh(\gamma_{ei}d_i)/\gamma_{ei}) & [S_{h1}] &= diag(\sinh(\gamma_{hi}d_i)/\gamma_{hi}) \\ [S_{e2}] &= diag(\gamma_{ei}\sinh(\gamma_{ei}d_i)) & [S_{h2}] &= diag(\gamma_{hi}\sinh(\gamma_{hi}d_i)) \end{aligned} \tag{2.47}$$

If one uses e_x, e_z and h_x, h_z to represent the components of $\bar{e}$ and $\bar{h}$ defined in equation (2.29), then from equation (2.1), the transverse electromagnetic field in the p^{th} layer can be expressed in the spectral domain as

$$\begin{aligned} e_x &= -\frac{\alpha}{\omega\varepsilon_0\varepsilon_r^p}\frac{\partial\psi^e}{\partial z} - \frac{\partial\psi^h}{\partial y} & -h_x &= -\frac{\partial\psi^h}{\partial y} + \frac{\alpha}{\omega\mu_0}\frac{\partial\psi^e}{\partial z} \\ e_z &= \frac{1}{j\omega\varepsilon_0\varepsilon_r^p}\left(\frac{\partial^2\psi^e}{\partial z^2} + \varepsilon_r^p k_0^2\psi^e\right) & jh_z &= \frac{1}{\omega\mu}\left(\frac{\partial^2\psi^h}{\partial z^2} + \varepsilon_r^p k_0^2\psi^h\right) \end{aligned} \tag{2.48}$$

Applying the non-equidistant discretization, equation (2.33), and the orthogonal transform, equation (2.40), the fields in the transform domain can be written in matrix notation as

$$\begin{aligned} \tilde{\underline{e}}_x &= -\frac{\alpha\delta_{he}}{\omega\varepsilon_0\varepsilon_r^p}\tilde{V}^e - \frac{\partial\tilde{V}^h}{\partial y} & -\tilde{\underline{h}}_x &= \left(-\frac{\partial\tilde{V}^h}{\partial y}\right) - \frac{\alpha\delta_{eh}}{\omega\mu_0}\tilde{V}^h \\ \tilde{\underline{e}}_z &= \frac{\varepsilon_r^p k_0^2 - \delta_{ee}}{j\omega\varepsilon_0\varepsilon_r^p}\tilde{V}^e & j\tilde{\underline{h}}_z &= \frac{\varepsilon_r^p k_0^2 - \delta_{hh}}{\omega\mu}\tilde{V}^h \end{aligned} \tag{2.49}$$

where

$$\begin{aligned} \tilde{\underline{e}}_x &= \left[T^h\right]^{-1}\left[r_h\right]^{-1}\tilde{e}_x & \tilde{\underline{h}}_x &= \left[T^e\right]^{-1}\left[r_e\right]^{-1}\tilde{h}_x \\ \tilde{\underline{e}}_z &= \left[T^e\right]^{-1}\left[r_e\right]^{-1}\tilde{e}_z & \tilde{\underline{h}}_z &= \left[T^h\right]^{-1}\left[r_h\right]^{-1}\tilde{h}_z \end{aligned} \tag{2.50}$$

Note that the vector formulation is introduced to represent the MoL discretization.

Using block matrix notation

$$\begin{bmatrix} \tilde{\underline{e}}_x \\ \tilde{\underline{e}}_z \\ j\tilde{\underline{h}}_z \\ -\tilde{\underline{h}}_x \end{bmatrix} = \left[R_p\right]\begin{bmatrix} \tilde{V}^e \\ \dfrac{\partial\tilde{V}^h}{\partial y} \\ \dfrac{\partial\tilde{V}^e}{\partial y} \\ \tilde{V}^h \end{bmatrix} \tag{2.51}$$

where $[\mathbf{R}_p]$ is a $4N_z$ by $4N_z$ matrix

$$\left[R_p\right] = \begin{bmatrix} -\dfrac{\alpha\delta_{he}}{\omega\varepsilon_0\varepsilon_r^p} & -[I] & [0] & [0] \\ \dfrac{\varepsilon_r^p k_0^2 - \delta_{ee}}{j\omega\varepsilon_0\varepsilon_r^p} & [0] & [0] & [0] \\ [0] & [0] & [0] & \dfrac{\varepsilon_r^p k_0^2 - \delta_{hh}}{\omega\mu} \\ [0] & [0] & -[I] & -\dfrac{\alpha\delta_{eh}}{\omega\mu_0} \end{bmatrix} \tag{2.52}$$

By combining equation (2.45) and equation (2.51), the field relationship between two layers is

$$\begin{bmatrix} \tilde{e}_x \\ \tilde{e}_z \\ j\tilde{h}_z \\ -\tilde{h}_x \end{bmatrix}_{y_k} = \left[R_p\right]\left[Q_p\right]\left[R_p\right]^{-1} \begin{bmatrix} \tilde{e}_x \\ \tilde{e}_z \\ j\tilde{h}_z \\ -\tilde{h}_x \end{bmatrix}_{y_m} \tag{2.53}$$

The expression for multiple layers can be obtained by cascading the respective matrices.

With equation (2.53) one can always transform the electromagnetic field from one layer to another. By transforming fields into the layers of metallization and applying the boundary conditions at those interfaces, a matrix equation similar to equation (2.6) and equation (2.15) can be obtained

$$\begin{bmatrix} \tilde{e}_x \\ \tilde{e}_z \end{bmatrix} = [Z] \begin{bmatrix} \tilde{j}_x \\ \tilde{j}_z \end{bmatrix} \tag{2.54}$$

$[Z]$ is a $2N_z$ by $2N_z$ matrix. Transforming the electric fields and currents back into the original domain by using the same orthogonal transform introduced in equation (2.40), the spectral domain algebraic matrix equation becomes

$$\begin{bmatrix} \tilde{e}_x \\ \tilde{e}_z \end{bmatrix} = [Z] \begin{bmatrix} \tilde{j}_x \\ \tilde{j}_z \end{bmatrix} \tag{2.55}$$

where [Z] is a $2N_z$ by $2N_z$ matrix

$$[Z] = \begin{bmatrix} [r_h][T^h] & [0] \\ [0] & [r^e][T^e] \end{bmatrix} [Z] \begin{bmatrix} [T^h]^{-1}[r_h]^{-1} & [0] \\ [0] & [T^e]^{-1}[r_e]^{-1} \end{bmatrix} \tag{2.56}$$

In summary, the following transforms have been utilized in the above analysis

$\rightarrow$ *Fourier transform* $\rightarrow$ *non-equidistant discretization* $\rightarrow$ *orthogonal transform*

i.e. $$\Psi^{e,h} \rightarrow \psi^{e,h} \rightarrow \left(\tilde{\psi}^{e,h} \rightarrow \tilde{\varphi}^{e,h} \right) \rightarrow \tilde{V}^{e,h} \tag{2.57}$$

$$(E_{x,y} \rightarrow e_{x,y}) \rightarrow (\tilde{e}_{x,y} \rightarrow \underset{\sim}{\tilde{e}}_{x,y})$$
$$(J_{x,y} \rightarrow j_{x,y}) \rightarrow \left(\tilde{j}_{x,y} \rightarrow \underset{\sim}{\tilde{j}}_{x,y} \right)$$

The system equation (2.55) is obtained by following the reverse procedure.

In summary, equation (2.1) to (2.57) represent the generalized procedure of the Space (from the MoL)-Spectral Domain (from the SDM) Approach (SSDA). Although in this chapter, the formulation is limited to a resonator problem, the foundation of the SSDA for scattering parameter calculation, which will be discussed in Chapter 3 and Chapter 4, is laid.

2.4.3 The Eigenvalue Solution of a Resonator Problem

The resonant frequency of a planar resonator can be calculated by finding the roots of the determinant of the system equation [17].

Galerkin's technique is applied to obtain the characteristic matrix equations. The

first step is to expand the elements of unknown $\hat{j}_x$ and $\hat{j}_z$ in terms of known basis functions with unknown coefficients a_{xi}^{l} and a_{zi}^{l}

$$j_{xi} = \sum_{l=1}^{N_x} a_{xi}^{l}\eta_{xi}^{l} \qquad j_{zi} = \sum_{l=0}^{N_x-1} a_{zi}^{l}\eta_{zi}^{l} \tag{2.58}$$

where l represents the l^{th} basis function, N_x is the total number of basis functions, i represents the i^{th} line and

$$\begin{aligned}\eta_{xi}^{l} &= w_i\left(J_0\left(\frac{w_i\alpha}{2}+l\pi\right)-J_0\left(\frac{w_i\alpha}{2}-l\pi\right)\right)\\ \eta_{zi}^{l} &= w_i\left(J_0\left(\frac{w_i\alpha}{2}+l\pi\right)+J_0\left(\frac{w_i\alpha}{2}-l\pi\right)\right)\end{aligned} \tag{2.59}$$

where w_i is the strip width. J_0 is the 0^{th} order Bessel's function. Or, in vector notation

$$\vec{\eta}_x^{\,l} = \begin{bmatrix}\eta_{x1}^{l}\\ \cdots\\ \eta_{xN_z}^{l}\end{bmatrix} \qquad \vec{\eta}_z^{\,l} = \begin{bmatrix}\eta_{z1}^{l}\\ \cdots\\ \eta_{zN_z}^{l}\end{bmatrix} \tag{2.60}$$

Calculating the inner product between basis functions and each element of the system equation (2.55) (further details can be found in Chapter 3) yields

$$\int_{-\alpha}^{\infty}\begin{bmatrix}\hat{e}_x\cdot\vec{\eta}_x^{\,l}\\ \hat{e}_z\cdot\vec{\eta}_z^{\,l}\end{bmatrix}d\alpha = \int_{-\infty}^{\infty}\left([Z]\begin{bmatrix}\hat{j}_x\\ \hat{j}_z\end{bmatrix}\right)\cdot\begin{bmatrix}\vec{\eta}_x^{\,l}\\ \vec{\eta}_z^{\,l}\end{bmatrix}d\alpha \qquad l = 1, 2, \ldots, N_x \tag{2.61}$$

the right side of equation (2.61) is always zero. The left side can be written as

$$[F(f)]\hat{a} = 0 \tag{2.62}$$

$[F(f)]$ is the result of the inner product and $\hat{a}$ represents the coefficient vector. f denotes the resonance frequency which can be obtained by solving the zeros of the determinant

$$det\left([F(f)]\right) = 0 \tag{2.63}$$

To extend the SSDA to calculate the S-parameters of planar discontinuities the deterministic quasi-static SSDA and the full-wave SSDA with hybrid boundary conditions are introduced in Chapter 4 and 5, respectively.

Chapter 3

The Quasi-Static SSDA

3.1 Why Quasi-static ?

Quasi-static numerical techniques are traditionally faster than full-wave techniques in particular on the serial machines widely used today. These methods do not benefit from the availability of parallel processors. For some applications their accuracy can rival that of full-wave techniques and, therefore, they are very useful engineering analysis tools. In the recent literature, the quasi-static analysis has again received more attention [21 - 24], because MMIC's and MHMIC's are usually small in dimension compared with the operating wavelength and, therefore, dispersion is normally weak. In [21] a quasi-static spectral domain approach (SDA) was used to calculate microstrip discontinuities. This method is numerically efficient but requires complicated 2-D basis functions, which sometimes may be difficult to find. A quasi-static finite difference method (FDM) is described in [22] to analyze CPW discontinuities. This method can treat arbitrary discontinuities, but at the expense of large computer memory. In [23] the quasi-static method of lines (MoL) is employed to analyze cross-coupled planar multiconductor systems. This method does not use basis functions and is faster than the FDM but still requires significant amounts of memory and is difficult to apply to arbitrary discontinuities. The deterministic SSDA eliminates these problems and will be introduced in the next section.

3.2 The Quasi-static SSDA

This approach utilizes the basic idea behind the SSDA but avoids solving an eigenvalue problem by using a new deterministic technique instead. To minimize errors in the calculation of the capacitance parameters, the excess charge density [24] has been used and calculated in the space-spectral domain in one step via Galerkin's method. This approach

leads to an algebraic equation for the equivalent circuit parameters of the discontinuities and is computationally very stable, requires little memory space and is very fast on serial computers. This method is capable of treating arbitrarily shaped planar circuit discontinuities. Figure 3.1 illustrates the type of discontinuities this method has been applied to.

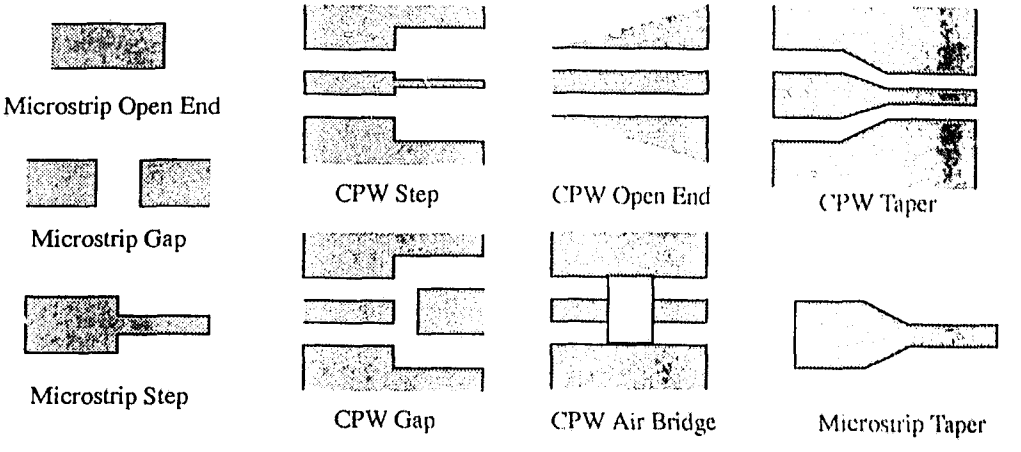

Figure 3.1 Planar circuit discontinuities

A CPW discontinuity illustrated in Figure 3.2 is used as an example to demonstrate the theory. This discontinuity contains three regions (1, 2, 3) with thicknesses h_1, h_2, h_3 and is shielded by a metal housing. The three regions are defined as:

1. $h_3+h_2<y<h_3+h_2+h_1$
2. $h_3<y<h_3+h_2$
3. $0<y<h_3$

As mentioned before, discretization of the structure in z-direction corresponds to slicing the structure in the x-y plane at each z-coordinate. Therefore, the potential for each slice must satisfy the 3-D Laplace's equation

$$\frac{\partial^2}{\partial x^2}\Psi + \frac{\partial^2}{\partial y^2}\Psi + \frac{\partial^2}{\partial z^2}\Psi = 0 \qquad (3.1)$$

In this case $k=0$ ($\omega=0$, compared with equation (2.2)). The task here is to simplify Laplace's equation which depends on the three spatial variables. The electric lines (solid lines) are introduced to represent a discretized electric potential ψ, which is independent

of the magnetic potential. The dashed lines are used to represent the magnetic potentials as used in the conventional MoL (the magnetic potential is not of interest here because it is independent of the quasi-static electric field). The shift in both lines is necessary to reduce the discretization error and can be derived from [8]. Similar to Chapter 2, the first step is to transform the electric potential function Ψ into ψ via a Fourier transform along the x-direction. Here the superscript is omitted because only the electric potential is of interest. The spatial variable x becomes a spectral variable α. The next step is to discretize ψ by using N_z lines in the z-direction which leads to the vector $\vec{\psi}$. The tapered region is enlarged in the left part of Figure 3.2, which demonstrates how a smooth transition is theoretically discretized and approximated by a sequence of abrupt steps.

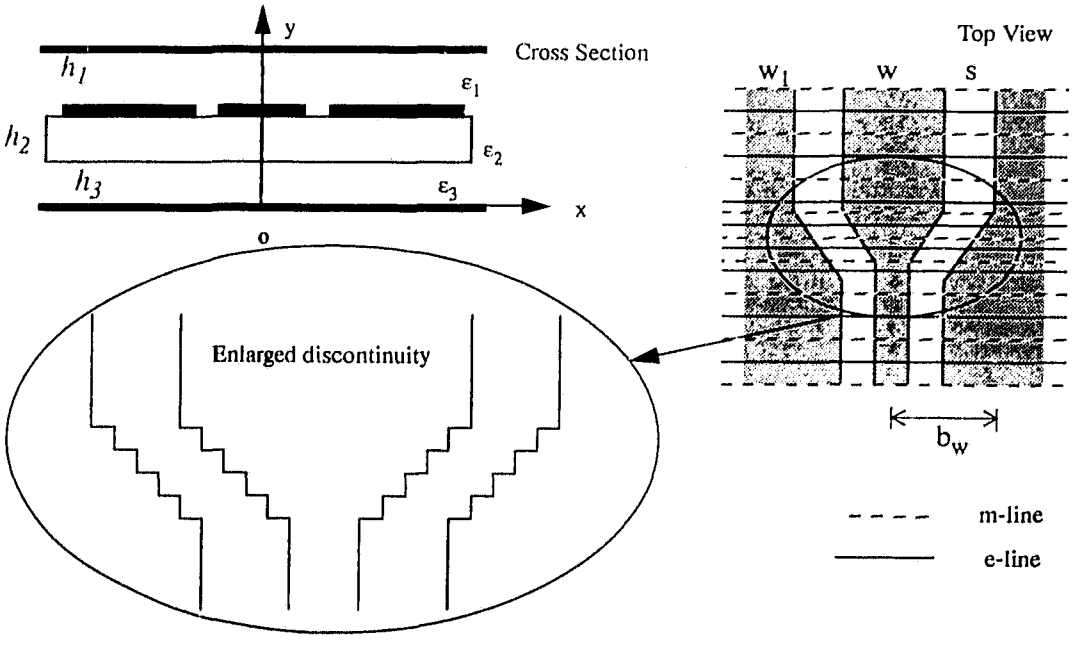

Figure 3.2 Discretization of a CPW discontinuity

By utilizing the basic steps of the SSDA in Chapter 2 with non-equidistant discretization in the z-direction, Laplace's equation can be decoupled

$$\frac{\partial^2 \vec{V}}{\partial y^2} - \gamma^2 \vec{V} = 0 \tag{3.2}$$

where

$$\gamma^2 = \delta^2 + \alpha^2 \qquad \hat{V} = [T]^t \hat{\varphi} \qquad \hat{\varphi} = [r_e]^{-1} \hat{\psi} \tag{3.3}$$

Due to the discretization, Laplace's equation (3.1) is now reduced to only one spatial variable, y. δ is the eigenvalue of $[D_{zz}]$. $[T]$ is the eigenvector matrix. δ and $[T]$ are defined in Chapter 2 (note: the superscript e is omitted here because only electric potentials are used in the formulation. γ has only two terms instead of three as in Chapter 2 because $k=0$). Solutions to the above 1-D simplified Laplace's equation can be expressed in terms of the sum of hyperbolic functions, and the relationship of the electric potentials between any two adjacent layers can be expressed in the same way as described in equation (2.42) of Chapter 2, that is

$$\begin{bmatrix} V_i \\ \dfrac{\partial V_i}{\partial y} \end{bmatrix}_{y_k} = \begin{bmatrix} \cosh\gamma_i d_i & \dfrac{1}{\gamma_i}\sinh\gamma_i d_i \\ \gamma_i \sinh\gamma_i d_i & \cosh\gamma_i d_i \end{bmatrix} \begin{bmatrix} V_i \\ \dfrac{\partial V_i}{\partial y} \end{bmatrix}_{y_m} \tag{3.4}$$

V_i is the i^{th} element of $\hat{V}$ and corresponds to the i^{th} line of discretization. Because equation (3.2) is decoupled, each line is represented by the same form of normal differential equation. Without loss of generality the subscript i can be removed in the following analysis. Instead, the subscript is now used to represent the potential in the different dielectric region.

For Laplace's equation, there is always $\gamma = \gamma_1 = \gamma_2 = \gamma_3$ because $k_{ij} = 0$ in equation (2.43).

The boundary condition at the interface is as follows:

$$\begin{aligned} V_1 &= V_2 \qquad at \qquad y = h_2 + h_3 \\ V_2 &= V_3 \qquad at \qquad y = h_3 \end{aligned} \tag{3.5}$$

$$\begin{aligned} \varepsilon_1 \frac{\partial V_1}{\partial y} - \varepsilon_2 \frac{\partial V_2}{\partial y} &= -\frac{q}{\varepsilon_o} \qquad at \qquad y = h_2 + h_3 \\ \varepsilon_2 \frac{\partial V_2}{\partial y} &= \varepsilon_3 \frac{\partial V_3}{\partial y} \qquad at \qquad y = h_3 \end{aligned} \tag{3.6}$$

where q is the charge density in the transform domain. At the top and bottom metallization

$$V_1 = 0 \qquad at \qquad y = h_1 + h_2 + h_3$$
$$V_3 = 0 \qquad at \qquad y = 0 \tag{3.7}$$

Substitute equation (3.7) into equation (3.4) yields

$$\frac{\partial V_2}{\partial y} = -\frac{\gamma}{\tanh \gamma h_2} V_2 \qquad at \qquad y = h_2 + h_3$$
$$\frac{\partial V_3}{\partial y} = \frac{\gamma}{\tanh \gamma h_3} V_3 \qquad at \qquad y = h_3 \tag{3.8}$$

Combine equation (3.4) - (3.8) provides

$$g(\gamma) V_1 = \frac{q}{\varepsilon_o} \tag{3.9}$$

where

$$g(\gamma) = \frac{\varepsilon_2 \gamma}{\tanh \gamma h_2} + \frac{\varepsilon_1 \gamma}{\tanh \gamma h_1} - \frac{\left(\frac{\varepsilon_2 \gamma}{\tanh \gamma h_2} \right)^2}{\frac{\varepsilon_2 \gamma}{\tanh \gamma h_2} + \frac{\varepsilon_3 \gamma}{\tanh \gamma h_3}} \tag{3.10}$$

To characterize a discontinuity, one needs to find the solution for the electric charge belonging to the discontinuity part. This is usually achieved by subtracting the total charge of the discontinuity area and the charge belonging to the connected transmission line. Since both quantities are often quite small, the errors arising from the subtraction of two electric charges, which are close in magnitude, can be significant. To avoid these errors, the excess charge technique [24] is used. This technique can briefly be summarized as follows: the 2-D transmission line problem is solved first in the spectral domain on either side of the discontinuity, i.e. solving equation (3.2) (homogeneous transmission line in z-direction) and analytically subtracting the charge distribution of the fictitious homogeneous transmission line from the charge distribution of the corresponding discretization line of the transmission line containing the discontinuity. Based on the above formulation, the 2-D problem can be solved by using the solution given in equation (3.9) with $\delta = 0$, i.e. $\gamma = \alpha$

$$g(\alpha)\, V_1 = \frac{q_o}{\varepsilon_o} \tag{3.11}$$

where q_o is the charge density of a fictitious homogeneous transmission line. The excess charge density ρ is defined as

$$\rho = q - q_o \tag{3.12}$$

Now the excess charge technique is applied, which means the two quantities $g(\gamma)$ and $g(\alpha)$ are subtracted

$$V_1 = (g(\gamma) - g(\alpha))^{-1} \frac{\rho}{\varepsilon_o} \tag{3.13}$$

and the results are transformed back into the original domain

$$\vec{\psi} = [G]\,\vec{\sigma} \tag{3.14}$$

$\vec{\sigma}$ is the excess charge vector in the original domain and

$$[G] = [r_h][T]\, diag\left[g(\gamma) - q(\alpha)\right]^{-1} [T]^t [r_h]^{-1} \tag{3.15}$$

where $diag[g(\gamma)-g(\alpha)]$ includes the difference $[g(\gamma)-g(\alpha)]$ from all the lines. The size of the matrix is N_z by N_z.

Galerkin's technique is now applied to obtain the characteristic matrix equation. The first step is to expand the elements of the unknown $\vec{\sigma}$ in terms of known basis functions with unknown coefficients a_i^l

$$\vec{\sigma} = \begin{bmatrix} \sigma_1 \\ \dots \\ \sigma_{N_z} \end{bmatrix} \qquad \sigma_i = \sum_{l=1}^{N_x} a_i^l \eta_i^l \qquad i = 1, \dots, N_z \tag{3.16}$$

where N_x is the number of basis functions, N_z is the number of discrete lines and

$$\eta_i^l = \int_{-\infty}^{\infty} \xi_i^l e^{j\alpha x}\, dx \tag{3.17}$$

η_i^l and ξ_i^l are Fourier transform pairs of basis functions. For CPW circuits, they take on the following form for the center conductor with width w_i (also for microstrip circuits with width w_i)

$$\xi_i^l = \frac{\cos\left[(2l-1)\pi\frac{x}{w_i}\right]}{\sqrt{1-\left(\frac{2x}{w_i}\right)^2}} \qquad l = 1, 2, \ldots \tag{3.18}$$

$$\eta_i^l = \frac{\pi w_i}{4}\left[J_o\left(\frac{\alpha w_i}{2} + (l-1)\pi\right) + J_o\left(\frac{\alpha w_i}{2} - (l-1)\pi\right)\right] \qquad l = 1, 2, \ldots \tag{3.19}$$

For (CPW) ground (symmetrical) conductors (w_{1i} is the ground conductor width, b_{wi} is the x-coordinate of the ground conductor center (one side))

$$\xi_i^l = \underbrace{\frac{\cos\left[l\pi\frac{(x+b_{wi})}{w_{1i}}\right]}{\sqrt{1-\left(\frac{2(x+b_{wi})}{w_{1i}}\right)^2}}}_{x<0} + \underbrace{\frac{\cos\left[l\pi\frac{(x-b_{wi})}{w_{1i}}\right]}{\sqrt{1-\left(\frac{2(x+b_{wi})}{w_{1i}}\right)^2}}}_{x>0} \qquad l = 0, 2, \ldots$$

$$\xi_i^l = \underbrace{\frac{\sin\left[l\pi\frac{(x+b_{wi})}{w_{1i}}\right]}{\sqrt{1-\left(\frac{2(x+b_{wi})}{w_{1i}}\right)^2}}}_{x<0} - \underbrace{\frac{\sin\left[l\pi\frac{(x-b_{wi})}{w_{1i}}\right]}{\sqrt{1-\left(\frac{2(x-b_{wi})}{w_{1i}}\right)^2}}}_{x>0} \qquad l = 1, 3, \ldots \tag{3.20}$$

$$\eta_i^l = -\frac{\pi w_{1i}}{2}\cos\alpha b_{wi}\left[J_o\left(\frac{\alpha w_{1i} + l\pi}{2}\right) + J_o\left(\frac{\alpha w_{1i} - l\pi}{2}\right)\right] \qquad l = 0, 2, \ldots$$

$$\eta_i^l = -\frac{\pi w_{1i}}{2}\sin\alpha b_{wi}\left[J_o\left(\frac{\alpha w_{1i} + l\pi}{2}\right) - J_o\left(\frac{\alpha w_{1i} - l\pi}{2}\right)\right] \qquad l = 1, 3, \ldots \tag{3.21}$$

For different microstrip or CPW discontinuities, one only needs to adjust w_i, b_{wi}

and w_{li} of each line instead of changing the form of the basis function. Thus the discontinuity shape can be **arbitrary**. This is an advantage of the SSDA and makes it possible to develop contour driven software.

Similar to Chapter 2, the inner product between basis functions and each element of the system equation (3.14) is calculated

$$\int_{-\alpha}^{\infty} \vec{\psi} \cdot \vec{\eta}^{l} d\alpha = \int_{-\infty}^{\infty} \left([G] \vec{\sigma} \right) \cdot \vec{\eta}^{l} d\alpha \qquad l = 1, 2, \ldots, N_x \tag{3.22}$$

In quasi-static analysis, the excitation potential is always a constant across the metallization. This property can be utilized to achieve a simple deterministic solution through the use of Parseval's theorem

$$\int_{-\infty}^{\infty} \vec{\psi} \cdot \vec{\eta}^{l} d\alpha = 2\pi \int_{-\infty}^{\infty} \vec{\Psi} \cdot \vec{\xi}^{l} dx \tag{3.23}$$

where

$$\vec{\eta}^{l} = \begin{bmatrix} \eta_1^{l} \\ \ldots \\ \eta_{N_z}^{l} \end{bmatrix} \qquad \vec{\xi}^{l} = \begin{bmatrix} \xi_1^{l} \\ \ldots \\ \xi_{N_z}^{l} \end{bmatrix} \tag{3.24}$$

$\vec{\Psi}$ is the discretized electric potential (inverse Fourier transform of $\vec{\psi}$) and is constant across the metallization. If this constant is defined as V_e, the left side of equation (3.22), which is further processed in equation (3.23), can be written as

$$\int_{-\infty}^{\infty} \vec{\psi} \cdot \vec{\eta}^{l} d\alpha = 2\pi V_e \int_{-\infty}^{\infty} \vec{\xi}^{l} dx = 2\pi V_e \vec{\eta}^{l} \Big|_{\alpha = 0} \tag{3.25}$$

Unlike the full-wave resonator analysis described in Chapter 2, the left side of system Equation (3.22) is known as an algebraic equation. The deterministic solution can be obtained by matrix inversion. Rewriting equation (3.22) in matrix form, which contains N_x independent equations, will yield

$$2\pi V_e \left[\begin{matrix} \vec{\eta}^{\,1} \\ \cdots \\ \vec{\eta}^{\,N_x} \end{matrix}\right]\Bigg|_{\alpha=0} = \int_{-\infty}^{\infty} \left(\left[\begin{matrix} \left([G]\vec{\sigma} \right) \cdot \vec{\eta}^{\,1} \\ \cdots \\ \left([G]\vec{\sigma} \right) \cdot \vec{\eta}^{\,N_x} \end{matrix}\right] \right) d\alpha \tag{3.26}$$

By using equation (3.16) and replacing the continuous integral by a discrete summation, equation (3.26) can be written as

$$\vec{\theta} = [Z]\vec{a} \tag{3.27}$$

where

$$\vec{\theta} = \frac{2\pi V_e}{\Delta\alpha} \left[\begin{matrix} \vec{\eta}^{\,1} \\ \cdots \\ \vec{\eta}^{\,N_x} \end{matrix}\right]\Bigg|_{\alpha=0} \qquad [Z] = Block\{[Z]_{km}\} \tag{3.28}$$

$$[Z]_{km} = \sum_{\alpha} \begin{bmatrix} G_{km}\eta_m^1\eta_m^1 & G_{km}\eta_m^2\eta_m^1 & \cdots & G_{km}\eta_m^{N_x}\eta_m^1 \\ G_{km}\eta_m^1\eta_m^2 & G_{km}\eta_m^2\eta_m^2 & \cdots & G_{km}\eta_m^{N_x}\eta_m^2 \\ \cdots & \cdots & \cdots & \cdots \\ G_{km}\eta_m^1\eta_m^{N_x} & G_{km}\eta_m^2\eta_m^{N_x} & \cdots & G_{km}\eta_m^{N_x}\eta_m^{N_x} \end{bmatrix} \tag{3.29}$$

$\Delta\alpha$ is the step width of the discrete Fourier integration. [Z] is a N_zN_x by N_zN_x block matrix, which contains N_z by N_z submatrices. Each submatrix $[Z]_{km}$ is a N_x by N_x matrix. G_{km} is the *(k, m)* element of [G].

The charge density coefficient vector $\vec{a}$ is defined as

$$\vec{a} = \left[a_1^1\ a_1^2\ \cdots\ a_1^{N_x}\ a_2^1\ a_2^2\ \cdots\ a_2^{N_x}\ \cdots\ a_{N_z}^1\ a_{N_z}^2\ \cdots\ a_{N_z}^{N_x} \right]^t \tag{3.30}$$

From equation (3.27), it is evident that only a one step matrix inversion is now required

$$\hat{a} = [Z]^{-1}\hat{0} \tag{3.31}$$

In contrast to finding zeros of a determinant through an iterative procedure (equation (2.63)), the quasi-static SSDA is a deterministic approach and provides the results by a one-time matrix inversion.

The total charge Q can be obtained by integrating the charge density over the discontinuity area

$$Q = \int\left[\int \hat{\sigma} e^{-j\alpha x} d\alpha\right] \cdot d\hat{S} \tag{3.32}$$

The equivalent circuit for different discontinuities is shown in Figure 3.3. The gap discontinuity is characterized by a π network. Open end, step in width, tapered discontinuities and air bridge are approximated by a shunt capacitor. The capacitances C_{p1}, C_{p2}, C_s or C_p are then calculated from $C=Q/V_e$ assuming different excitation voltages V_e (even mode $V_{e1}=1$, $V_{e2}=1$, odd mode $V_{e1}=1$, $V_{e2}=-1$ for a π network, $V_e=1$ for a shunt capacitor) at both ports of the strip. $V_e=0$ is chosen for the ground conductor. The s-parameters can be derived by using network theory.

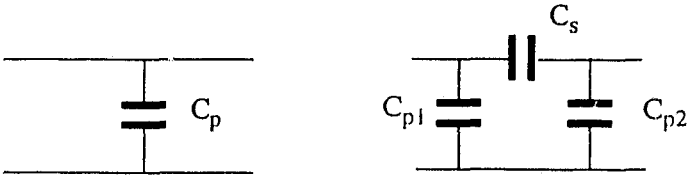

Step, Open End
Airbridge

Gap

Figure 3.3 The equivalent circuit

To calculate the shunt capacitance of an air bridge, the above formulation must be slightly modified. A CPW air bridge is shown in Figure 3.4.

The three region formulation from equation (3.2) to equation (3.31) can still be utilized if the air bridge is approximated as a patch sitting above the CPW as shown in Figure 3.4. This approximation is only valid when h_2 is very small (h<w/5), which is true in most cases. Also the boundary condition of equation (3.6) is changed to

$$\varepsilon_1 \frac{\partial V_1}{\partial y} - \varepsilon_2 \frac{\partial V_2}{\partial y} = -\frac{q_1}{\varepsilon_o} \qquad at \qquad y = h_2 + h_3$$
$$\varepsilon_2 \frac{\partial V_2}{\partial y} - \varepsilon_3 \frac{\partial V_3}{\partial y} = -\frac{q_2}{\varepsilon_o} \qquad at \qquad y = h_3 \tag{3.33}$$

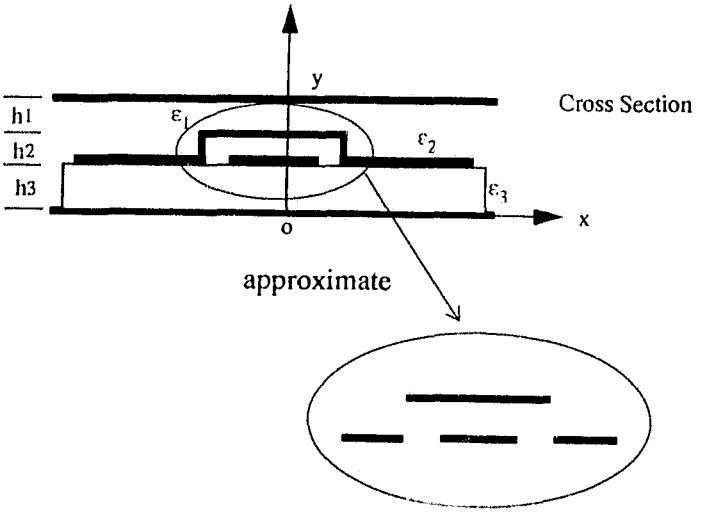

Figure 3.4 A CPW Air Bridge

Where q_1 is the charge density (in the transformed domain) of the bridge and q_2 is the charge density of the CPW area. Following a procedure similar to that described by equations (3.5) - (3.15), a new system equation can be derived

$$[g(\gamma)] \begin{bmatrix} V_1 \\ V_2 \end{bmatrix} = \begin{bmatrix} q_1 \\ q_2 \end{bmatrix} \tag{3.34}$$

where

$$\left[g(\gamma)\right] = \varepsilon_o \begin{bmatrix} \dfrac{\varepsilon_2\gamma}{\tanh\gamma h_2} + \dfrac{\varepsilon_1\gamma}{\tanh\gamma h_1} & \dfrac{-\varepsilon_2\gamma}{\tanh\gamma h_2} \\ \dfrac{-\varepsilon_2\gamma}{\tanh\gamma h_2} & \dfrac{-\varepsilon_2\gamma}{\tanh\gamma h_2} + \dfrac{\varepsilon_3\gamma}{\tanh\gamma h_3} \end{bmatrix} \tag{3.35}$$

Finally the system equation in the transform domain has the same form as equation (3.14), but in a block matrix formulation. $[G]$ from equation (3.15) becomes

$$\left[G\right] = \begin{bmatrix} \left[r_h\right]\left[T\right] & 0 \\ 0 & \left[r_h\right]\left[T\right] \end{bmatrix} diag\Big(\left[g(\gamma)\right] - \left[g(\alpha)\right]\Big)^{-1} \begin{bmatrix} \left[r_h\right]^{-1}\left[I\right]' & 0 \\ 0 & \left[r_h\right]^{-1}\left[I\right]' \end{bmatrix} \tag{3.36}$$

Each submatrix is a 2x2 matrix. The total rank of [G] is $2N_z$ by $2N_z$.

3.3 On the Nature of the SSDA

It has been shown in Chapter 2 that the MoL and SDM are indeed equivalent if the same discretization scheme is used, i.e., the number of lines in the MoL equals the number of spectral terms in the SDM. This equivalency forms the basis of the SSDA. After having introduced the quasi-static SSDA, it is worthwhile to look back and study the nature of the SSDA. This section will show that by using a TE_y/TM_y formulation, the SSDA includes the 2-D SDM and 2-D MoL.

In the analysis of planar transmission line problems the most common approach is to express the electromagnetic field in terms of E_z and H_z (i.e, TE_z and TM_z wave), which gives a coupled TE_z and TM_z wave formulation as described in Chapter 2. But when the field is expressed in terms of E_y and H_y, a transmission line type of formulation can be obtained by coordinate rotation (in the x-z plane) to a u-v coordinate system, which, for the SDM, led to the immittance approach [4] or a simplified formulation in the MoL [13], [25]. If a TE_y and TM_y wave formulation is used in the SSDA, some interesting results can be obtained.

Starting from Maxwell's equations

$$\nabla\times\vec{E} = -j\omega\mu\vec{H}$$
$$\nabla\times\vec{H} = j\omega\varepsilon\vec{E} \tag{3.37}$$

and rearranging the above equation yields a more suitable form for the purpose of this section

$$\left(\frac{\partial^2}{\partial y^2}+k^2\right)\begin{bmatrix}E_x\\E_z\end{bmatrix} = \begin{bmatrix}\frac{\partial^2}{\partial x\partial y} & j\omega\mu\frac{\partial}{\partial z}\\ \frac{\partial^2}{\partial y\partial z} & -j\omega\mu\frac{\partial}{\partial x}\end{bmatrix}\begin{bmatrix}E_y\\H_y\end{bmatrix}$$
$$\left(\frac{\partial^2}{\partial y^2}+k^2\right)\begin{bmatrix}H_x\\H_z\end{bmatrix} = \begin{bmatrix}-j\omega\varepsilon\frac{\partial}{\partial z} & \frac{\partial^2}{\partial y\partial z}\\ -j\omega\varepsilon\frac{\partial}{\partial z} & \frac{\partial^2}{\partial x\partial y}\end{bmatrix}\begin{bmatrix}E_y\\H_y\end{bmatrix} \tag{3.38}$$

A variable transformation in x- and z- direction (this can be either the Fourier transform of the SDM or the orthogonal transform of the MoL) is now introduced as follows

$$\frac{\partial}{\partial x}\rightarrow -j\alpha_x \qquad \frac{\partial}{\partial z}\rightarrow -j\alpha_z$$
$$\frac{\partial^2}{\partial x^2}\rightarrow -\alpha_x^2 \qquad \frac{\partial^2}{\partial z^2}\rightarrow -\alpha_z^2 \tag{3.39}$$

Using the lower case to represent the field components after the transform, equation (3.38) is written as a decoupled TE/TM to y formulation

$$\begin{bmatrix}e_u\\e_v\end{bmatrix} = \begin{bmatrix}0 & -\omega\mu\\ -j\frac{\partial}{\partial y} & 0\end{bmatrix}\begin{bmatrix}e_y\\h_y\end{bmatrix} \qquad \begin{bmatrix}h_u\\h_v\end{bmatrix} = \begin{bmatrix}\omega\varepsilon & 0\\ 0 & -j\frac{\partial}{\partial y}\end{bmatrix}\begin{bmatrix}e_y\\h_y\end{bmatrix} \tag{3.40}$$

where

$$\begin{bmatrix} e_u \\ e_v \end{bmatrix} = U \begin{bmatrix} e_x \\ e_z \end{bmatrix} \qquad \begin{bmatrix} h_u \\ h_v \end{bmatrix} = U \begin{bmatrix} h_x \\ h_z \end{bmatrix}$$

$$U = \frac{1}{\sqrt{\alpha_x^2 + \alpha_z^2}} \begin{bmatrix} -\alpha_z & \alpha_x \\ \alpha_x & \alpha_z \end{bmatrix} \tag{3.41}$$

α_x and α_z can be spectral terms or eigenvalues of the transform matrix, depending on which method is used in the x- and z-direction, respectively (note: when an eigenvalue is used, it should be multiplied by j). The U matrix corresponds to the coordinate rotation from (x, z, y) to (u, v, y) as shown in Figure 3.5.

Based on the above formulation, the SSDA is really a 2-D SDM when α_x and α_z are spectral terms. Similarly, the SSDA becomes a 2-D MoL when α_x and α_z are eigenvalues of the transform matrices (discretization). In the SSDA the SDM and MoL can be applied separately to the x- and z-direction, respectively, or one can use any one of the two methods. It is worthwhile to point out that the reason behind the formulation is that the TE_y and TM_y modes are independent (not coupled anymore!). On the other hand, this equivalency is only valid from the formulation point of view. The SSDA has its unique style in solving discontinuity problem because it uses neither 2-D discretization as in the MoL nor 2-D basis function as in the SDM.

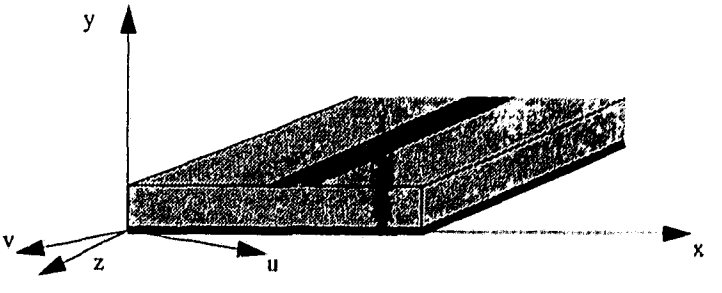

Figure 3.5 Configuration of general transmission line

In summary

- The SSDA combines the MoL and SDM which can be derived from each other
- The SSDA can be formulated from the TE_y/TM_y wave expansion using a coordinate rotation.
- the 2-D SDM or 2-D MoL are the special case of a general hybrid method: the SSDA.

Chapter 4

The Full-wave SSDA

This chapter focuses on the full-wave SSDA. Two alternative approaches are presented: an eigenvalue and a deterministic approach.

The foundation of the full-wave SSDA is laid in chapter 2, where only a homogeneous boundary condition is used. To calculate the S-parameters of planar circuits, inhomogeneous boundary conditions must be included. This chapter describes two different approaches to implement the inhomogeneous boundary conditions and to extract S-parameters.

4.1 Eigenvalue Approach

The eigenvalue approach employs the concept of self-consistent inhomogeneous (or hybrid) boundary conditions at the end of feed lines which are connected to either side of the discontinuity. This approach makes it possible to simulate the whole structure via an eigenvalue equation in which the solution is the reflection coefficient of the discontinuity. The hybrid boundary conditions have been used before in [15] and [16], but in the first case to model the forward and reflected waves individually and in the second case to find the total field at the launching point by using a modal source approach. In the method presented here, the reflection coefficient (or S_{11}) is obtained directly.

If a 2-port discontinuity (Figure 4.1) is under investigation, it is assumed that at some distance from port 1 of the discontinuity, there will be a standing wave of the fundamental mode only consisting of incident and reflected waves:

$$\psi^{e} = \psi_{o}^{e}\left(e^{-j\beta_1 z} - re^{j\beta_1 z}\right)$$
$$\psi^{h} = \psi_{o}^{h}\left(e^{-j\beta_1 z} + re^{j\beta_1 z}\right) \tag{4.1}$$

where β_1 is the propagation constant at the boundary of port 1 calculated separately by using the SDM, r is the voltage reflection coefficient and ψ^{e}_{o}, ψ^{h}_{o} are the incident TE/TM potentials at $z = 0$, which are solutions of the homogeneous connecting transmission line.

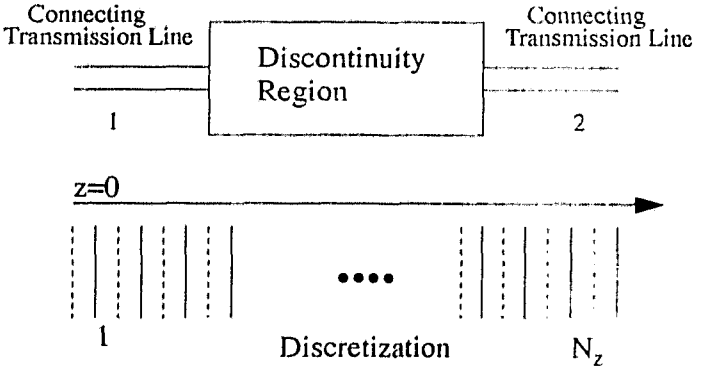

Figure 4.1 An eigenvalue approach

The inhomogeneous boundary (z-direction) conditions can be derived independently without considering the spectral domain factors (x-direction). With reference to the matched, open- and short-circuited conditions, at port 2 three different cases for the boundaries exist, these are the Dirichlet, Neumann and hybrid boundary conditions. For the matched condition at port 2, there are two choices for the discretization scheme depending on whether to assign an e or h line as the first line. In the following, the discretization scheme begins with an m (magnetic)-line (open-circuit). When using an m-line as first line, only the boundary condition for ψ^{h}_{o} is specially treated, while the boundary condition for ψ^{e}_{o} is implicitly included. For the same reason, only the bound-

ary condition for ψ_o^h is specially treated when using an e-line as the first line.

In case of the matched and open-circuit conditions, the hybrid boundary condition at port 1 can be expressed as:

$$\frac{\partial \psi^h}{\partial z} = -j\beta_1\left(e^{-j\beta_1 z} - re^{j\beta_1 z}\right)\psi_o^h \tag{4.2}$$

and at $z = 0.5\ h$

$$\psi_1^h = \left(e^{-j0.5h\beta_1} + re^{j0.5h\beta_1}\right)\psi_o^h \tag{4.3}$$

combining equation (4.2) and equation (4.3)

$$\left.\frac{\partial \psi^h}{\partial z}\right|_{z=0.5h} = -j\beta_1 \frac{e^{-j0.5h\beta_1} - re^{j0.5h\beta_1}}{e^{-j0.5h\beta_1} + re^{j0.5h\beta_1}}\psi_1^h \tag{4.4}$$

equation (4.4) can be simplified as

$$\left.\frac{\partial \psi^h}{\partial z}\right|_{z=0.5h} = u\psi_1^h \tag{4.5}$$

where

$$u = -j\beta_1 \frac{1 - j\tau\tan(0.5h\beta_1)}{\tau - j\tan(0.5h\beta_1)} \qquad \tau = \frac{1+r}{1-r} \tag{4.6}$$

The voltage reflection coefficient r is thus explicitly involved in the hybrid boundary conditions. At port 2 the matched condition corresponds to:

$$\frac{\partial \psi^e}{\partial z} = -j\beta_2 \psi_{N_z}^e \tag{4.7}$$

where β_2 is the propagation constant at port 2 if a two-port circuit is considered. The propagation constants β_1 and β_2 can be derived from the 1-D SDM or MOL. Note that the matched condition corresponds to the discretization scheme of the open-circuit condition. In a similar way, the hybrid boundary conditions obtained for the short-circuit situation is as follows:

$$\left.\frac{\partial \psi^{e}}{\partial z}\right|_{z=(Nz+0.5)h} = -v\psi_1^{e} \tag{4.8}$$

where

$$v = j\beta_1 \frac{\tau - j\tan(0.5h\beta_1)}{1 - j\tau\tan(0.5h\beta_1)} \qquad \tau = \frac{1+r}{1-r} \tag{4.9}$$

Obviously, the potential functions and their first derivatives constitute the characteristic solutions of the whole circuit. It is interesting to see that the complex functions of the inhomogeneous boundary conditions at the input described in the above equations are not only expressed in terms of the propagation constant β_1 but also in terms of the discretization interval h and the unknown voltage reflection coefficient r (or s_{11}). In other words, the inhomogeneous boundary conditions are no longer "static" and strongly depend on the unknown scattering parameter, which in turn depends on the geometry of the structure of interest as well as the operating frequency. This is why the inhomogeneous boundary conditions are said to be self-consistent.

In summary, when the load of port 2 is matched, open or short, the corresponding boundary conditions are listed in the following table (homo=homogeneous boundary condition, inhomo=inhomogeneous boundary condition)

port 2	ψ^{e}_1	ψ^{h}_1	ψ^{e}_2	ψ^{h}_2
matched	*homo*	*inhomo*	*inhomo*	*homo*
open	*homo*	*inhomo*	*homo*	*homo*
short	*inhomo*	*homo*	*homo*	*homo*

Table 4.1. Boundary conditions

It is noted that only the case of inhomogeneous boundary condition need to be specially treated here, because the case of homogeneous boundary condition is discussed in Chapter 2. Similar to Chapter 2, the determinant equation will be derived from the SSDA procedure. The solution of this determinant equation is the unknown reflection coefficient r. The matched condition is taken as an example in the following analysis. The inhomogeneous boundary conditions are

$$\left.\frac{\partial \psi^{h}}{\partial z}\right|_{z=0.5h} = u\psi_{1}^{h}$$
$$\left.\frac{\partial \psi^{e}}{\partial z}\right|_{z=(Nz+0.5)h} = -v\psi_{Nz}^{e} \tag{4.10}$$

in which u and v are the coefficients defined in equation (4.6) and (4.9). In order to maintain the essential transformation properties (known from the MOL procedure), symmetric second-order finite-difference operators are required to deal with the Helmholtz equation and, in particular, the field equations tangential to the interfaces. Using the concept and algorithm described in Chapter 2, the electric and magnetic potential vectors in the original discrete domain are normalized by diagonal matrices:

$$\hat{\Phi}^{e,h} = \left[r_{e,h}\right]^{-1}\hat{\Psi}^{e,h} \tag{4.11}$$

with

$$\left[r^{e}\right] = \begin{bmatrix} \sqrt{uh} & & \\ & 1 & \\ & & \ddots \\ & & & 1 \end{bmatrix} \qquad \left[r^{h}\right] = \begin{bmatrix} 1 & & \\ & \ddots & \\ & & 1 \\ & & & \sqrt{vh} \end{bmatrix} \tag{4.12}$$

Therefore, the first and second derivatives of the potential functions are approximated by formulae similar to the ones in Chapter 2. Note that the unknown voltage reflection coefficient r is directly involved in the first element of $[r^{e,h}]$ and its related matrices.

Applying the continuity condition at each dielectric interface leads to a matrix relationship between the tangential field components of two adjacent subregions in the interface plane. Next, by successively utilizing the continuity condition and multiplying the resulting matrices by the transmission line matrices associated with the multilayer subregions, the boundary conditions from the top and bottom walls can be transformed into the interface plane of the discontinuity. This leads to a kind of space-spectral Green's function in the transform domain which must be transformed back into the original domain. This step can be performed by the conventional MoL and SDA procedures independently. From the mathematical viewpoint there is no difference which procedure is applied first. However, applying the MoL first leads to a better physical understanding and easier mathematical treatment. As a result, the matrix elements of the resulting

Green's function in the space-spectral domain are once again coupled to each other through the reverse transformation back into the original domain

$$\begin{bmatrix} \tilde{e}_x \\ \tilde{e}_z \end{bmatrix} = [Z] \begin{bmatrix} \tilde{J}_x \\ \tilde{J}_z \end{bmatrix} \tag{4.13}$$

Galerkin's technique is again used together with an appropriate choice of basis functions which will be defined on the conductor surface for each slicing line in the z-direction. This leads to a characteristic matrix equation system which must be solved for the zeros of its determinant, whereby the determinant is a function of the reflection coefficient r.

$$det\Big([F(r)] \Big) = 0 \tag{4.14}$$

For irregularly shaped discontinuities, the geometric parameters become a function of the z-coordinate and, therefore, are different for each line. In general, this does not complicate the analysis of planar structures at all, as long as the circuit contour can be described mathematically or by a set of coordinates. In addition, singularities of the circuit in the x-direction are automatically considered in the formulation of the basis functions. Once the voltage reflection coefficient r is known, an arbitrary constant for the first element of the x-oriented current coefficients can be assumed. Applying a singular value decomposition technique yields all the current coefficients for the chosen basis functions assigned to each discrete line. Therefore, the S-parameters can be extracted from incident and reflected currents on the strip.

4.2 Deterministic Approach

Although the eigenvalue approach for the full-wave SSDA has the advantages that no 2-D field distribution calculation is required, the root of the determinant, which is derived from a large matrix, must be found. For practical applications, a "one-step" solution is most desirable. In this section, a deterministic full-wave SSDA is presented, which avoids solving an eigenvalue equation by iterative computation.

A deterministic approach was used earlier in the 2-D MoL [12] [26]. In [12] a "three-step" approach was presented rather than a "one-step" approach because open and

short conditions were utilized. In [26] inhomogeneous boundary conditions were introduced. But based on the author's experience, the resulting algorithm does not provide a stable solution because a good matching condition for S-parameter calculation can not be realized.

The key steps in the following approach is to express the field distribution on the connecting transmission line (far from the discontinuity) as a superposition of incident and reflected waves, then derive the inhomogeneous boundary conditions for incident and reflected waves (similar to the previous section, the eigenvalue approach), and finally combine the incident and reflected waves to satisfy the tangential field condition at the metallization plane. By solving the 2-D transmission line problem first, the incident wave distribution is known. The reflected wave distribution is derived by using the knowledge of the incident wave.

Figure 4.2 illustrates the deterministic approach. Region B_1 and C together are called region B. Port 2 is always matched.

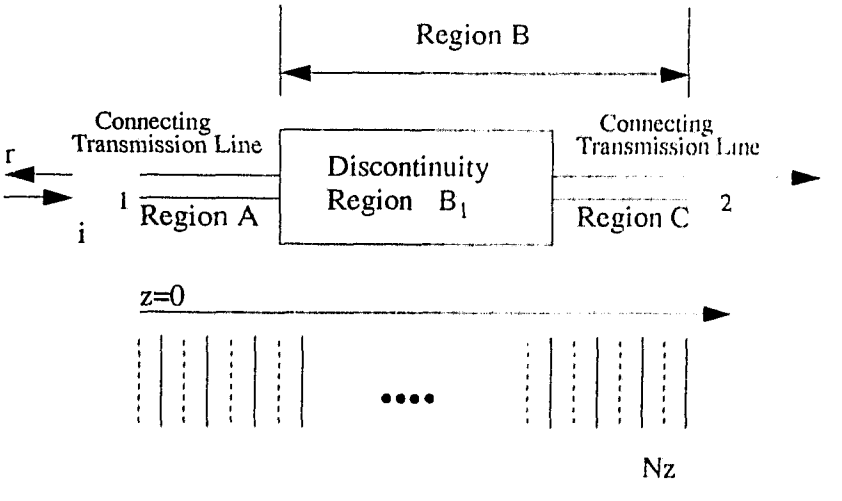

Figure 4.2 A deterministic approach

It is assumed that only one propagation mode exists on the transmission line connected to port 1, which is so far from the discontinuity region B_1, that the higher order modes excited by the discontinuity have vanished at port 1. The same assumption also applies to

region C. Using i and r to represent the incident and reflected waves, the inhomogeneous boundary conditions are expressed as

$$\begin{aligned} &incident \quad \left.\frac{\partial \psi^{h}}{\partial z}\right|_{z=0.5h} = -j\beta_1 e^{j\beta_1 0.5h}\psi_1^{h} \\ &reflected \quad \left.\frac{\partial \psi^{h}}{\partial z}\right|_{z=0.5h} = j\beta_1 e^{-j\beta_1 0.5h}\psi_1^{h} \end{aligned} \qquad \text{port1} \qquad (4.15)$$

$$\begin{aligned} &incident \quad \left.\frac{\partial \psi^{e}}{\partial z}\right|_{z=(Nz+0.5)h} = -j\beta_2 e^{-j\beta_2 0.5h}\psi_{Nz}^{e} \\ &reflected \quad \left.\frac{\partial \psi^{e}}{\partial z}\right|_{z=(Nz+0.5)h} = -j\beta_2 e^{-j\beta_2 0.5h}\psi_{Nz}^{e} \end{aligned} \qquad \text{port 2} \qquad (4.16)$$

Similar to equation (4.10), equation (4.15) and equation (4.16) can be simplified as

$$\begin{aligned} \left.\frac{\partial \psi^{h}}{\partial z}\right|_{z=0.5h}^{i,r} &= u^{i,r}\psi_1^{h} \\ \left.\frac{\partial \psi^{e}}{\partial z}\right|_{z=(Nz+0.5)h}^{i,r} &= -v\psi_{Nz}^{e} \end{aligned} \qquad (4.17)$$

where

$$u^{r} = j\beta_1 e^{-j\beta_1 0.5h} \qquad u^{i} = -j\beta_1 e^{j\beta_1 0.5h} \qquad v = -j\beta_2 e^{-j\beta_2 0.5h} \qquad (4.18)$$

As shown in Chapter 2, two system equations can be obtained for incident and reflected waves respectively

$$\begin{bmatrix} \mathcal{E}_x^{i} \\ \mathcal{E}_z^{i} \end{bmatrix} = [Z^{i}] \begin{bmatrix} \mathcal{N}_x^{i} \\ \mathcal{J}_z^{i} \end{bmatrix} \qquad \begin{bmatrix} \mathcal{E}_x^{r} \\ \mathcal{E}_z^{r} \end{bmatrix} = [Z^{r}] \begin{bmatrix} \mathcal{N}_x^{r} \\ \mathcal{J}_z^{r} \end{bmatrix} \qquad (4.19)$$

Rearranging equation (4.19) and using subscripts A and B to represent fields and currents in different regions, yields

$$\begin{bmatrix} \mathcal{E}_A^i \\ \mathcal{E}_B^i \end{bmatrix} = \begin{bmatrix} Z_{AB}^i \end{bmatrix} \begin{bmatrix} \mathcal{J}_A^i \\ \mathcal{J}_B^i \end{bmatrix} \qquad \begin{bmatrix} \mathcal{E}_A^r \\ \mathcal{E}_B^r \end{bmatrix} = \begin{bmatrix} Z_{AB}^r \end{bmatrix} \begin{bmatrix} \mathcal{J}_A^r \\ \mathcal{J}_B^r \end{bmatrix} \tag{4.20}$$

Once again Galerkin's technique is applied (described in chapter 2 and 3) to expand the unknown incident and reflected currents in terms of known basis functions η and unknown coefficients $C^{i,r}$

$$\mathcal{J}^{i,r} = \sum C^{i,r} \eta \tag{4.21}$$

Calculating the inner product of basis functions and using equation (4.20) yields

$$\begin{bmatrix} \begin{bmatrix} W_{11}^i \end{bmatrix} & \begin{bmatrix} W_{12}^i \end{bmatrix} \\ \begin{bmatrix} W_{21}^i \end{bmatrix} & \begin{bmatrix} W_{22}^i \end{bmatrix} \end{bmatrix} \begin{bmatrix} C_A^i \\ C_B^i \end{bmatrix} = \begin{bmatrix} \langle e_A^i, \eta_{BA} \rangle \\ \langle e_B^i, \eta_B \rangle \end{bmatrix} \tag{4.22}$$

$$\begin{bmatrix} \begin{bmatrix} W_{11}^r \end{bmatrix} & \begin{bmatrix} W_{12}^r \end{bmatrix} \\ \begin{bmatrix} W_{21}^r \end{bmatrix} & \begin{bmatrix} W_{22}^r \end{bmatrix} \end{bmatrix} \begin{bmatrix} C_A^r \\ C_B^r \end{bmatrix} = \begin{bmatrix} \langle e_A^r, \eta_A \rangle \\ \langle e_B^r, \eta_B \rangle \end{bmatrix} \tag{4.23}$$

$C^i{}_A$ is the known (from 2-D SDM) coefficient for the current distribution at the connecting transmission line at port 1 (region A), $C^r{}_A$ is the unknown coefficient of the reflected current distribution at port 1. Although i and r are used here, both $C^i{}_B$ and $C^r{}_B$ are the unknown coefficients of the outgoing current distribution at port 2.

In region A or B, on the metallization, the total tangential electric field must be zero

$$e^i + e^r = 0 \tag{4.24}$$

Combining equation (4.22), (4.23) and (4.24) yields

$$\begin{cases} \begin{bmatrix} W_{11}^i \end{bmatrix} C_A^i + \begin{bmatrix} W_{11}^r \end{bmatrix} C_A^r + \left(\begin{bmatrix} W_{12}^i \end{bmatrix} - \begin{bmatrix} W_{12}^r \end{bmatrix} \right) C_B^i + \begin{bmatrix} W_{12}^r \end{bmatrix} C_B^r = 0 \\ \begin{bmatrix} W_{21}^i \end{bmatrix} C_A^i + \begin{bmatrix} W_{21}^r \end{bmatrix} C_A^r + \left(\begin{bmatrix} W_{22}^i \end{bmatrix} - \begin{bmatrix} W_{22}^r \end{bmatrix} \right) C_B^i + \begin{bmatrix} W_{12}^r \end{bmatrix} C_B^r = 0 \end{cases} \tag{4.25}$$

where

$$C_B^{ir} = C_B^i + C_B^r \tag{4.26}$$

C^{ir}_B is more useful for determining the S-parameters. Since C^i_A is known, equation (4.25) can be solved by eliminating C^i_B,

$$\left(\left[W_{11}^r\right] - \left[W_i\right]\left[W_{21}^r\right]\right)C_A^r + \left(\left[W_{12}^r\right] - \left[W_i\right]\left[W_{22}^r\right]\right)C_B^{ir} = \left(\left[W_i\right]\left[W_{21}^i\right] - \left[W_{11}^i\right]\right)C_A^i \tag{4.27}$$

where

$$\left[W_i\right] = \left(\left[W_{12}^i\right] - \left[W_{12}^r\right]\right)\left(\left[W_{22}^i\right] - \left[W_{22}^r\right]\right)^{-1} \tag{4.28}$$

In equation (4.27), C^r_A and C^{ir}_B are unknown. Because C^{ir}_B is valid in region B_1 and C, equation (4.27) can be further simplified by replacing C^{ir}_B by the known coefficients of region C (solution of a homogeneous transmission line) multiplied by an unknown factor. Thus the number of unknowns is reduced to 1 in region C no matter how many lines are used there. Applying the same principle to region A will also reduce the number of unknowns in region A from N_A to 1.

Finally, C^r_A and C^{ir}_B can be obtained by simple matrix algebra which is described in the appendix.

Since the coefficients of the reflected current at port 1 and outgoing current at port 2 are known, the currents can be calculated accordingly. They are defined as I^-_1 and I^-_2. Also the incident current obtained from a 2-D SDM analysis is defined as I^+_1. The S-parameter can then be calculated by

$$S_{11} = \frac{I_1^-}{I_1^+} \tag{4.29}$$

$$S_{12} = \frac{I_2^-}{I_1^+}\sqrt{\frac{Z_2}{Z_1}} \tag{4.30}$$

where Z_i is the characteristic impedance of the connecting homogeneous transmission line at port i ($i=1, 2$).

Chapter 5

Numerical and Experimental Results

5.1 Convergence Analysis of Quasi-static SSDA

A convergence analysis is performed for a microstrip open-ended discontinuity, as shown in Figure 5.1 (ε_r is the dielectric constant and h is the thickness of the substrate). N_x is the number of basis functions in the x-direction. N_z is the number of lines in the z-direction. The convergence behavior depends on the number of spectral terms, Nz, and Nx. When the number of basis functions is increased, the number of spectral terms must be increased accordingly. A good convergence behavior is obtained when N_z >40, N_x>2, and the spectral term is greater than 80.

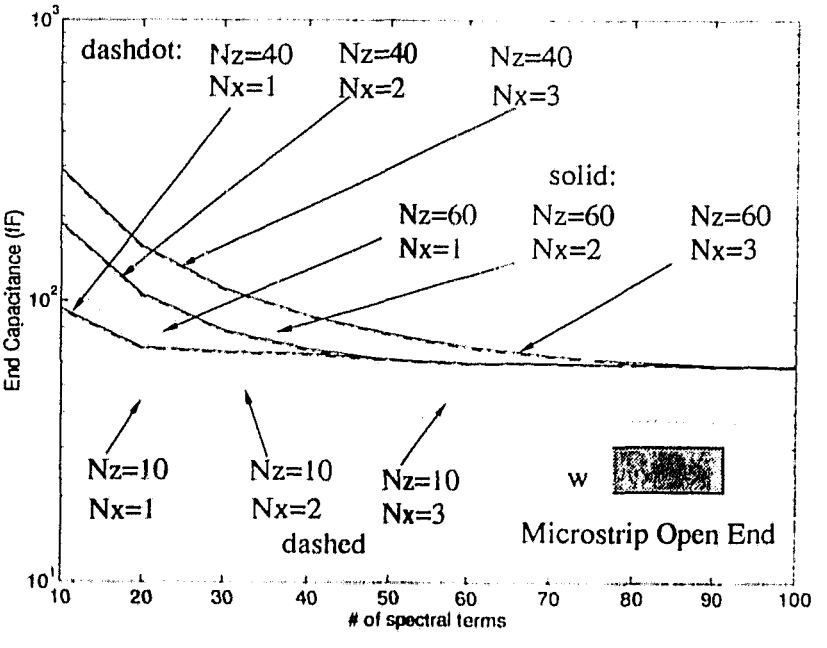

Figure 5.1 Convergence analysis of the Quasi-static SSDA ($w/h=1$, $\varepsilon_r=9.6$)

5.2 Simulation Results of Quasi-static SSDA

First of all the microstrip (MS) and CPW open end, gap and step in width as well as the CPW air bridge are analyzed by the quasi-static SSDA. Results are shown on Figure 5.2 to Figure 5.8. Those results are used to validate the SSDA.

Figure 5.2 shows the equivalent capacitance of a microstrip open end. The solid line is calculated by the SSDA. All markers are results from literature.

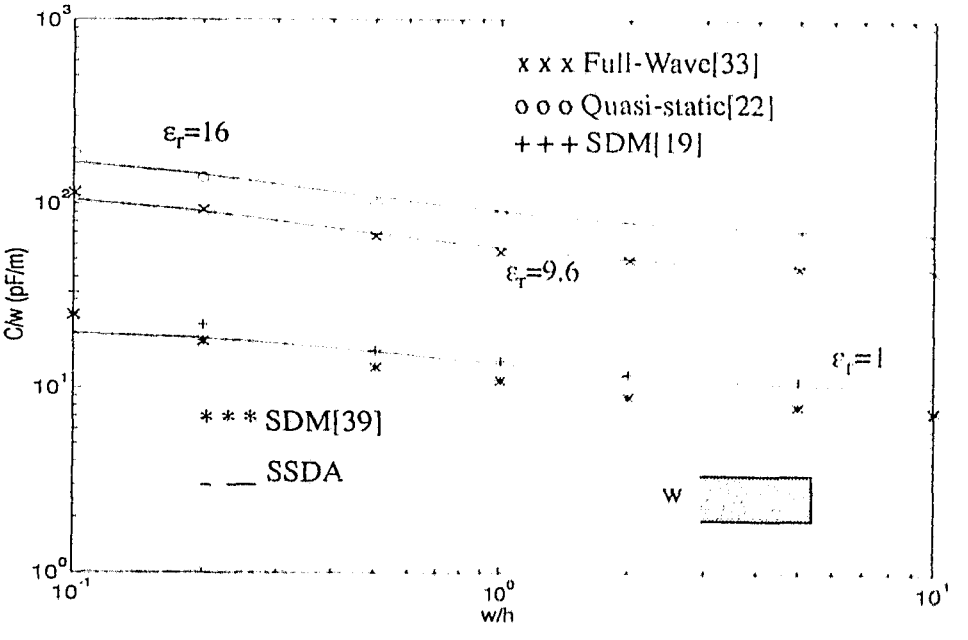

Figure 5.2 Capacitance of microstrip open ends.

Figure 5.3 shows the equivalent capacitances of a microstrip gap, which is represented by a π network as shown in Figure 3.3. The circles represent the SDM simulation and stars represent measurements [21]. The solid line is the results of the quasi-static SSDA simulation.

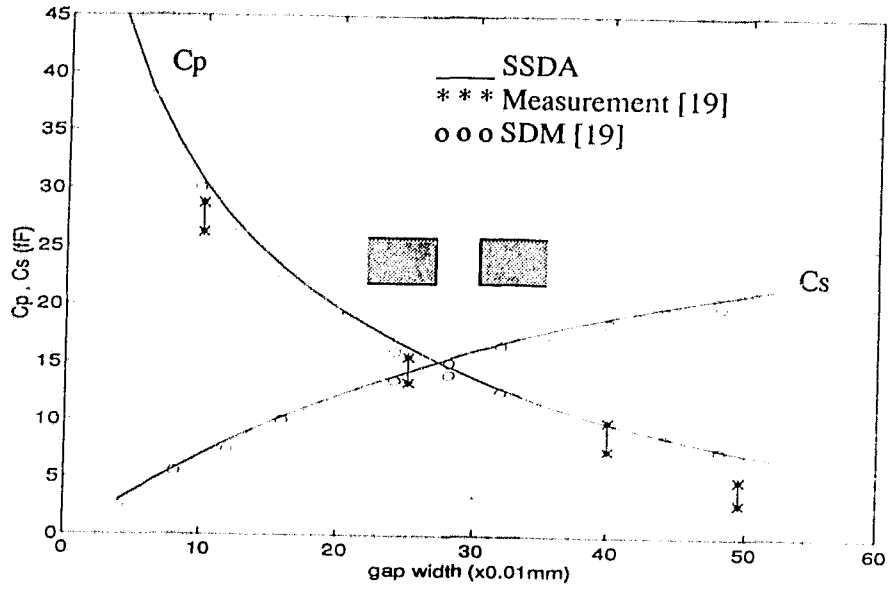

Figure 5.3 Equivalent capacitance of a microstrip gap discontinuity. w/h=1, h=0.508mm, ε_r=8.875

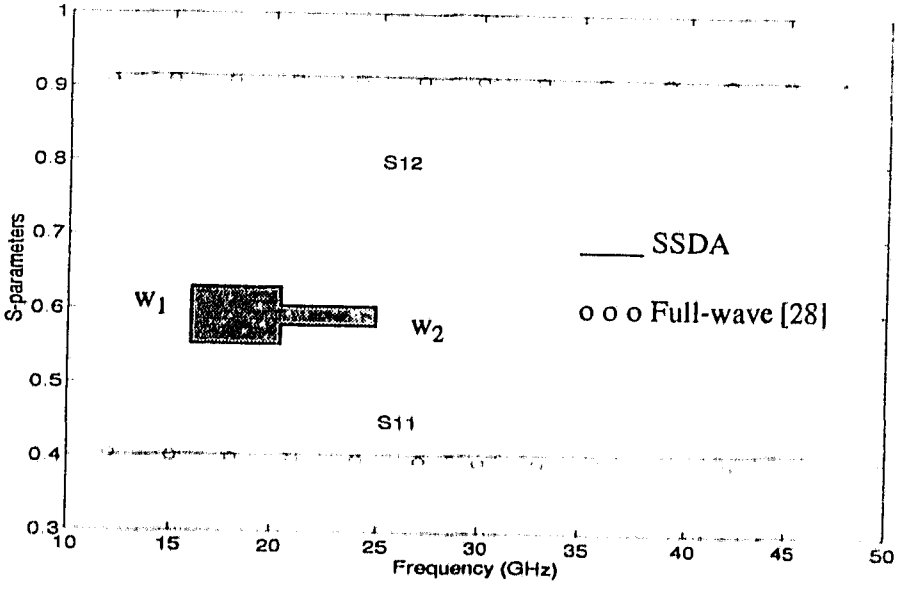

Figure 5.4 S-parameters of a microstrip step. w_1=1mm, w_2=0.25mm, w/h=1, ε_r=10.

Figure 5.4 illustrates the S-parameters of a microstrip step discontinuity, which was derived from network theory, and its shunt capacitance value. The circles represent the full-wave SDM simulation [30]. The solid line is calculated by the quasi-static SSDA.

Figure 5.5 presents the equivalent capacitance of an open-ended coplanar waveguide compared with published results. The solid line is calculated by the quasi-static SSDA. The circles and stars represent finite difference simulation and measurement [22], respectively.

Figure 5.6 shows the S-parameters for a coplanar air-bridge. The circles represent the results from a full-wave analysis using the Frequency Domain Finite Difference (FDFD) method [31].

Figure 5.7 illustrates the S-parameters of a CPW step discontinuity analyzed in [32]. The solid line is calculated by the SSDA. The circles are calculated by the full-wave SDM [32].

Figure 5.8 presents the S-parameters of a CPW gap analyzed in [22]. The solid line is calculated by the SSDA. The circles represent the results from the quasi-static SDM [22].

In summary, Figure 5.2 to Figure 5.8 present a variety of planar discontinuities. The SSDA simulation agrees well with either published results or measurements.

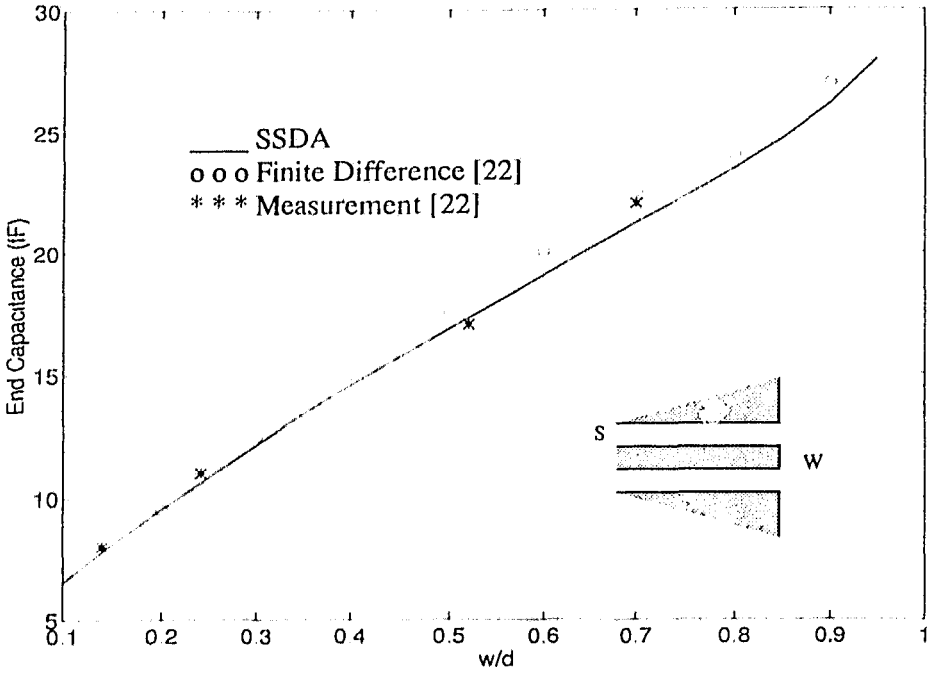

Figure 5.5 Equivalent capacitance of a CPW open end. ε_r=9.6, h=0.635, h/d=1, d=w+2s

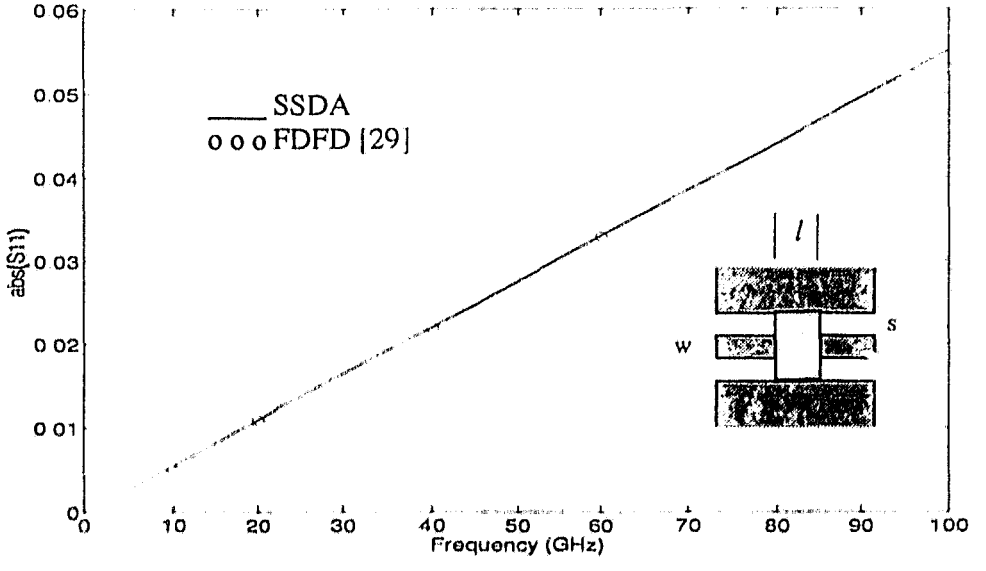

Figure 5.6 S-parameter of a CPW airbridge. w=15μm, s=10μm, l=3μm, h=200μm, b=3μm

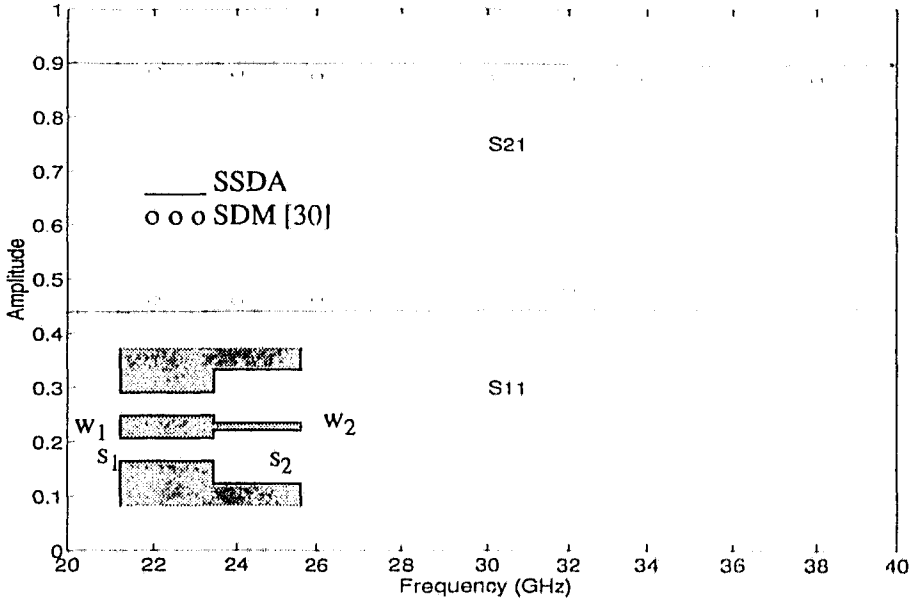

Figure 5.7 S-parameters of a CPW step. w_1=0.4mm, w_2=0.1mm, s_1=0.1mm, w_2=0.4mm, ε_r=9.8, h=0.254mm

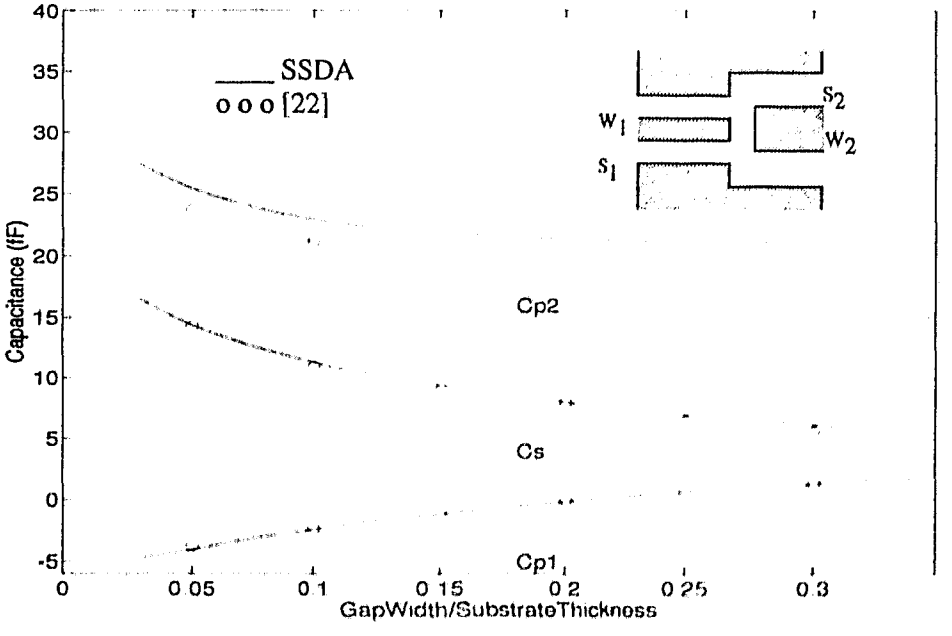

Figure 5.8 Equivalent capacitance of a CPW gap. d_1=2s_1+w_1, d_2=2s_2+w_2,ε_r=9.8, h=0.635mm, w_1/h=0.2, $w_1/d1$=$w_2/d2$=0.56, w_2/w_1=3

The main reason why the quasi-static SSDA works extremely well for MHMIC's is because the circuit dimensions are small compared with the wavelength, which means the dispersive effect is normally very small (the dispersive effect may become obvious at very high frequencies). When this condition is not valid (Figure 5.12), visible discrepancies to full-wave techniques may occur at lower frequencies.

The computation time of the quasi-static SSDA is typically a few minutes on a SUN SPARC-2 station (this will give the results over the whole frequency range). It is noteworthy to point out that results shown from Figure 5.2 to Figure 5.8 do not only demonstrate the good agreement with published results, but also show that this method is flexible. The accuracy of this deterministic quasi-static SSDA compares well with full-wave methods and measurements.

To show the ability of modeling arbitrary discontinuities, microstrip and CPW MHMIC tapered discontinuities are calculated. The transitions are represented by their equivalent capacitances as illustrated in Figure 5.9. When the length of the slope, Ws, increases, the equivalent capacitance decreases. This makes perfect physical sense. When the length of the slope equals zero, it represents an abrupt step in width (this was proved by calculating the capacitance of a step). The whole capacitance curve is quite smooth which shows the good numerical stability of this method.

The S-parameter of a CPW air bridge is also calculated in terms of air bridge length, which is shown in Figure 5.10. One can observe that when the air bridge length L decreases, S_{11} decreases too, because the capacitance to the ground decreases.

Figure 5.11 and Figure 5.12 show the limitation of the quasi-static SSDA. Figure 5.11 shows the S-parameters of a microstrip step discontinuity up to 100GHz. Although at frequencies below 50GHz the comparison with full-wave techniques is excellent, higher order modes start to propagate on this structure at 60GHz which is not accounted for in the quasi-static method. This leads to an increase of S_{11} and a decrease in S_{21} at about 50GHz.

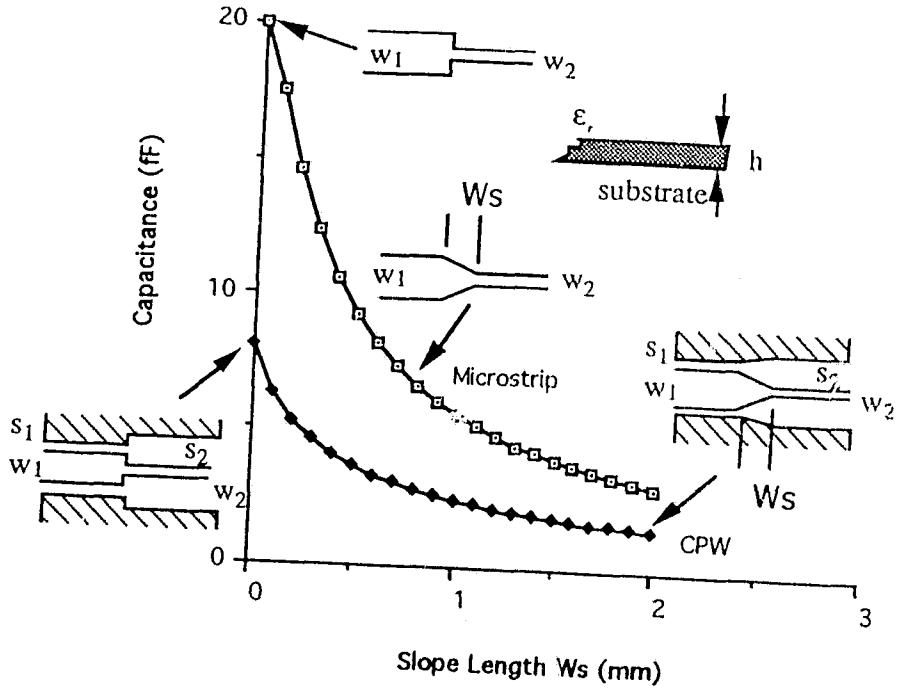

Figure 5.9 Equivalent capacitance of a microstrip and a CPW step/taper. For CPW, w_1=0.8mm, s_1=0.1mm, w_2=0.2mm, s_2==0.6mm, ε_r=9.6, h=0.254mm. For microstrip, w_1=1mm, w_2=0.25mm, ε_r=9.6, h=0.25mm

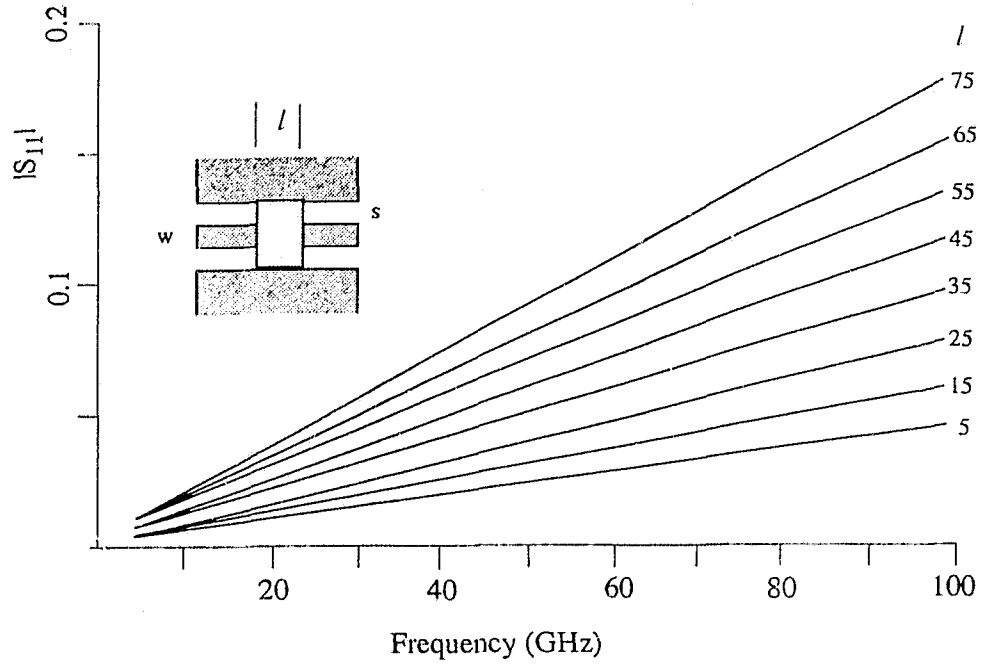

Figure 5.10 S-parameters of a CPW airbridge versus bridge length *l*. *w=0.3mm, s=0.1mm, b=3μm, ε_r=9.6, h=0.254mm.*

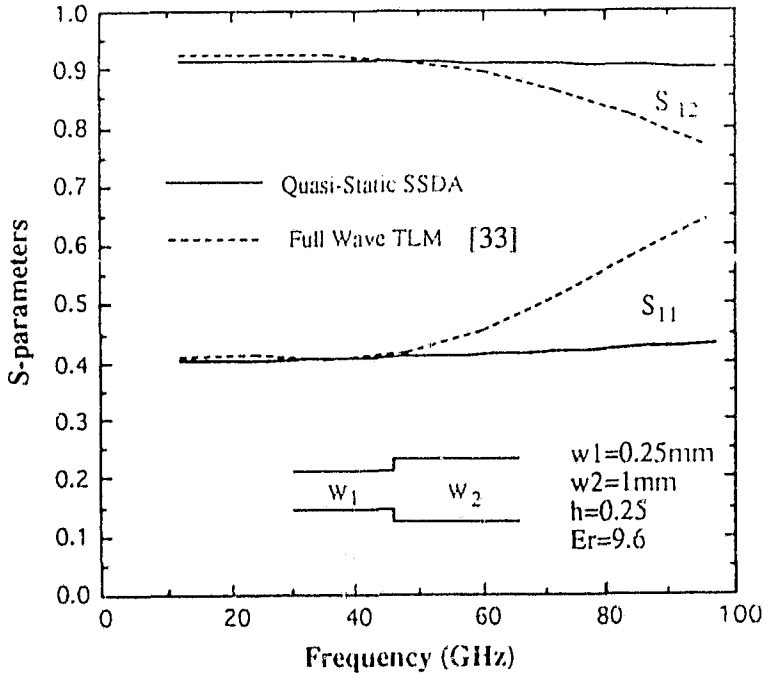

Figure 5.11 Frequency dependent behavior of microstrip step

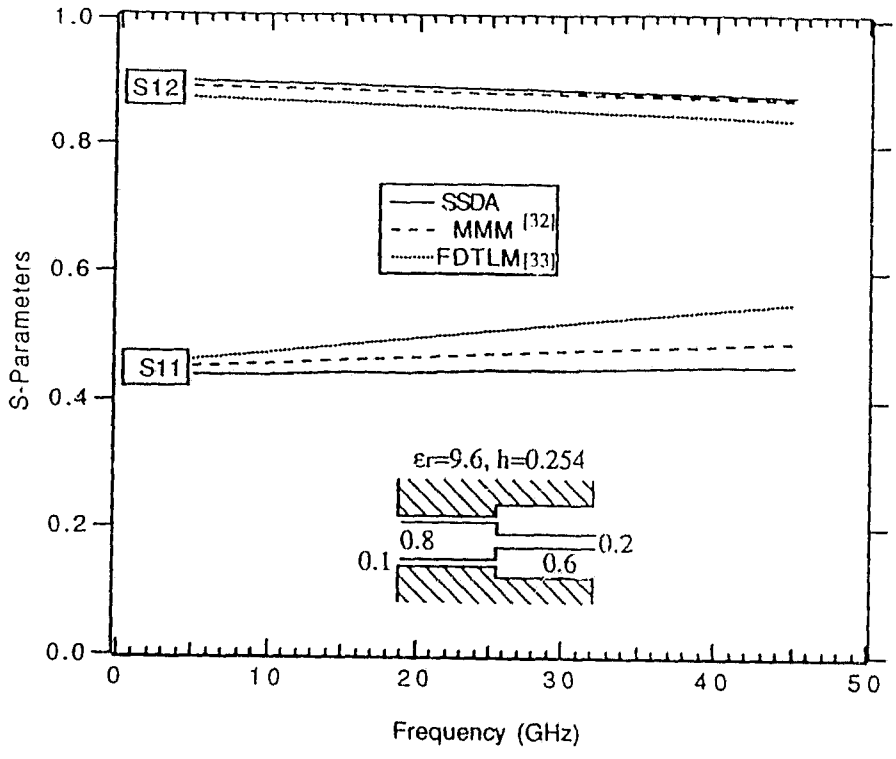

Figure 5.12 Frequency dependent behavior of CPW step

5.3 Convergence Study of Full-wave SSDA

A convergence analysis is performed for a microstrip step discontinuity as shown in Figure 5.13.

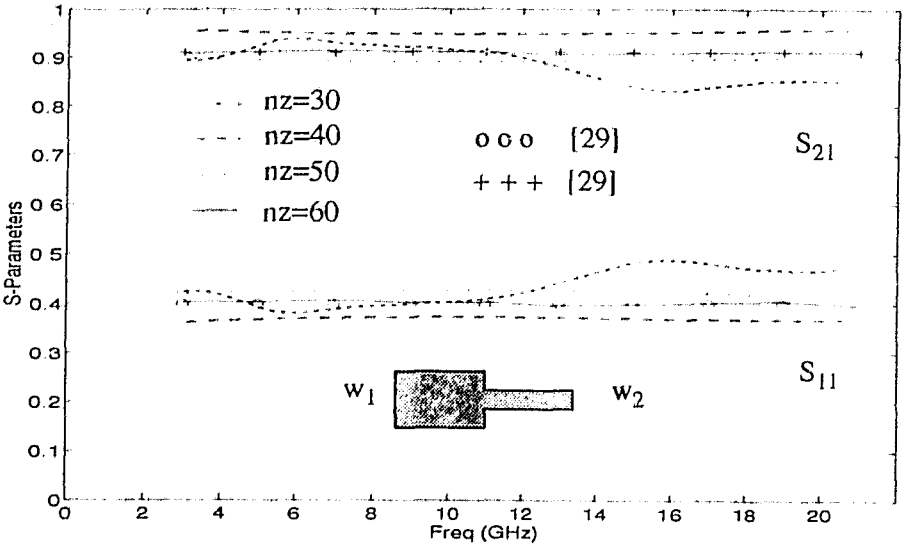

Figure 5.13 Convergency behavior of the full-wave SSDA
$w_1=1mm$, $w_2=0.25mm$, $h=0.25mm$, $\varepsilon_r=10$

When the number of lines (in the propagation direction z) is greater than 50, convergence is achieved.

As pointed out in Chapter 4, using the approach presented in [26] (using hybrid boundary conditions) will lead to an unstable solution, because the matching condition is applied to only one line. Using the full-wave SSDA, a stable solution can always be obtained.

5.4 Simulation Results of Full-wave SSDA

A comparison of S-parameters obtained by the full-wave SSDA and by others (i.e [30]) for a microstrip step discontinuity are shown in Figure 5.14 and Figure 5.15. A good agreement can be observed over the frequency range up to 20GHz.

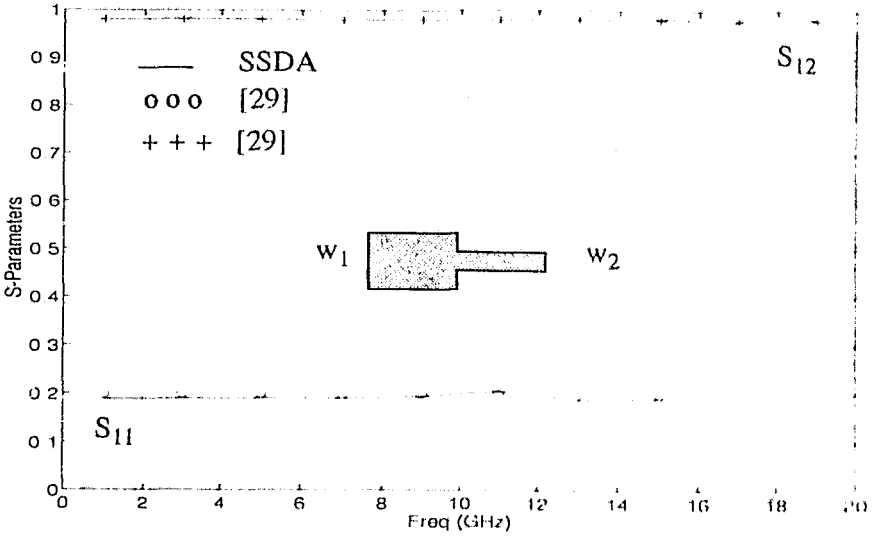

Figure 5.14 Full-wave S-parameters of a microstrip step
$w_1=1mm$, $w_2=0.5mm$, $h=0.25mm$, $\varepsilon_r=10$

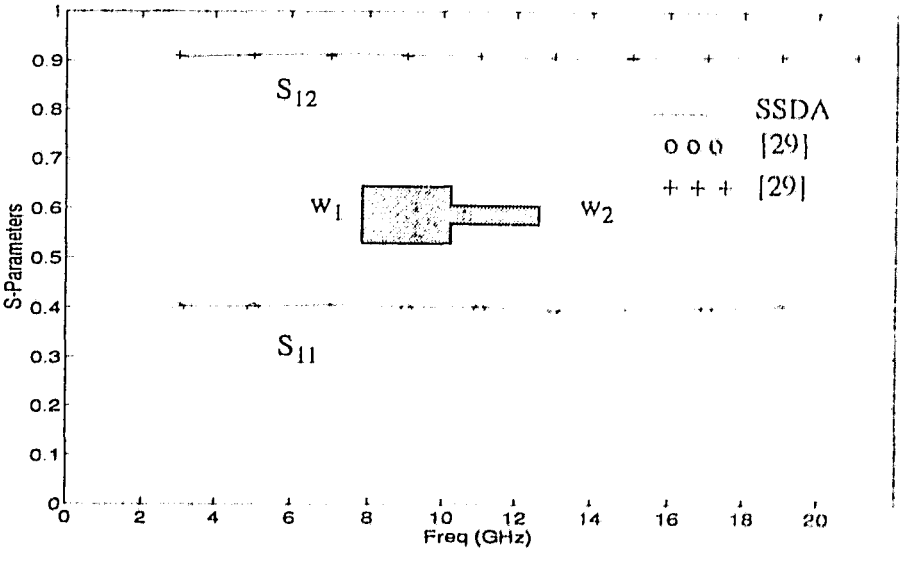

Figure 5.15 Full-wave S-parameters of a microstrip step
$w_1=1mm$, $w_2=0.25mm$, $h=0.25mm$, $\varepsilon_r=10$

Transmission characteristics of two closely spaced microstrip step discontinuities are shown Figure 5.16 (from 2 to 40 GHz). It is evident from the Figure 5.16 (a) that there is a strong interaction between both steps since their separation is less than half a guided wavelength. This type of structure is widely used in filter design. In general, it behaves like a low-pass filter as in the case of l=1.20mm. The interconnecting stub also contributes to the dip around 5GHz for the case of l=1.20mm. The shorter the length l, the further the dip moves towards higher frequencies (as shown in the case of l=0.15mm). Hence the stop band effect occurs only at higher frequencies. Also the Q factor decreases because the coupling between two homogeneous transmission lines increases. The phase characteristics of the S-parameters are shown in Figure 5.16(b).

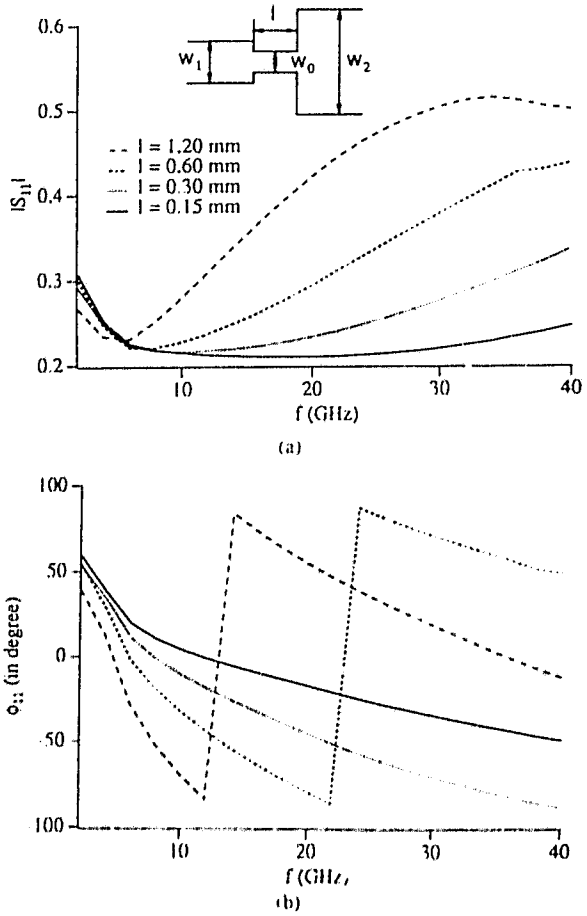

Figure 5.16 S-parameters for a cascaded step discontinuity separated by a transmission line of length l. w_1=0.4mm, wo=0.2mm, w_2=0.8mm, ε_r=3.8, h=0.25mm.
(a) Magnitude of S_{11}, (b) Phase of S_{11}

5.5 Experimental Results

By using a network analyzer at microwave and millimeter wave frequencies, it is often impossible to directly measure the scattering parameters of a device under test (DUT). De-embedding techniques must be used to obtain correct S-parameters [36 - 42].

Some MHMIC discontinuities have been fabricated for experimental investigation. Figure 5.17 to Figure 5.20 show the calculated (solid line) and measurement(dashed line) results performed at the University of Victoria. Five MHMIC's with via holes are tested. The de-embedded S-parameters are compared with quasi-static SSDA simulations. All MHMIC's are built on 0.254 mm conductor-backed substrate with dielectric constant 9.6. Ground plane via holes are used to suppress the microstrip mode. Figure 5.17 shows the S-parameters of a single CPW gap. Figure 5.18 investigates CPW double gaps with two different resonator lengths. The SSDA calculation shows how the resonant peaks move when the resonator length changes. Figure 5.18 illustrates the S-parameters of a CPW step discontinuity.

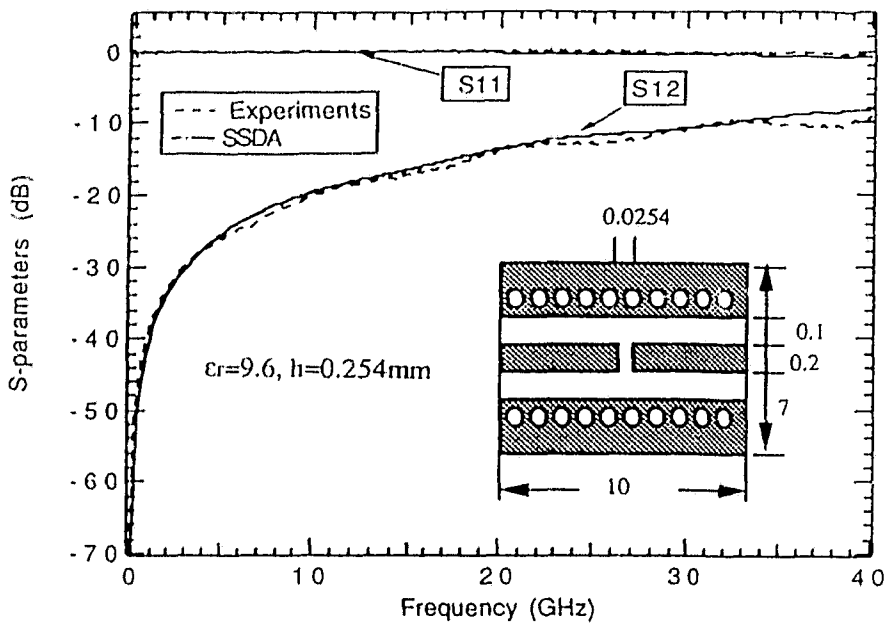

Figure 5.17 Measured and computed S-parameters of a CPW gap

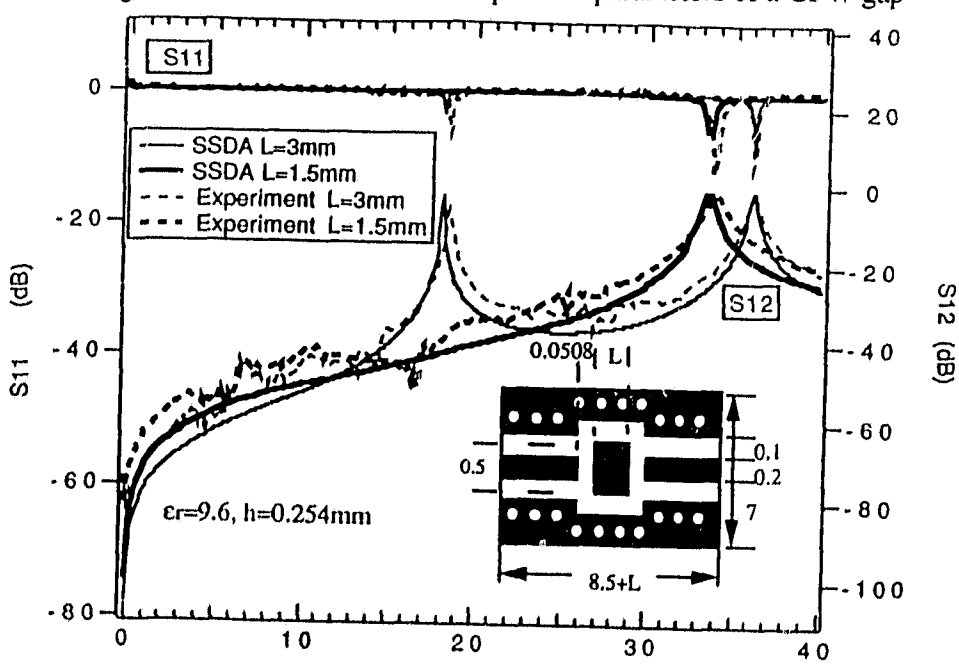

Figure 5.18 Measured and computed S-parameters of end-coupled CPW resonators

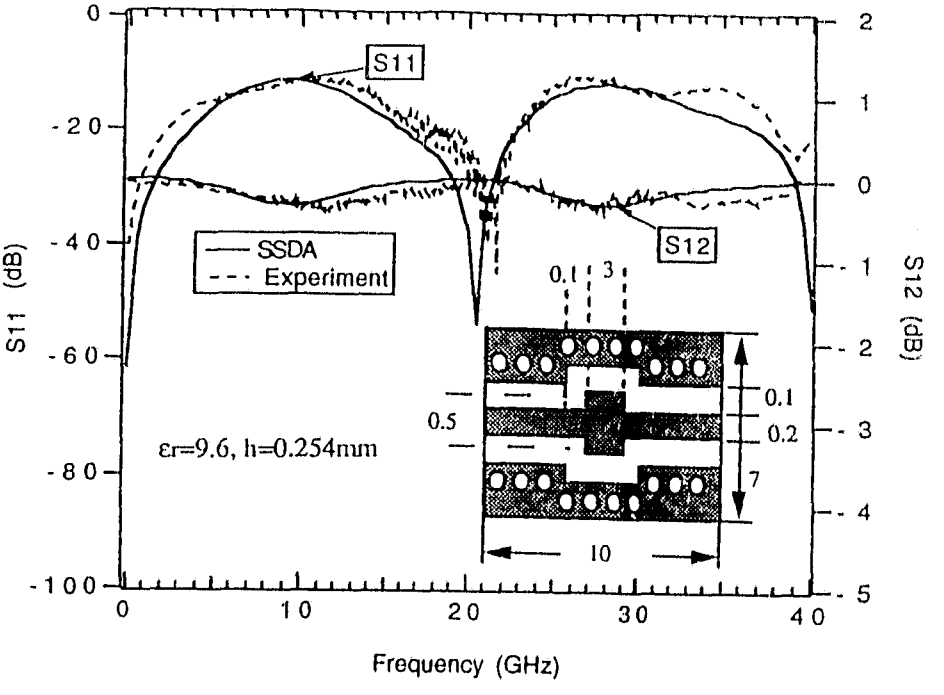

Figure 5.19 Measured and computed S-parameters of a CPW step discontinuity

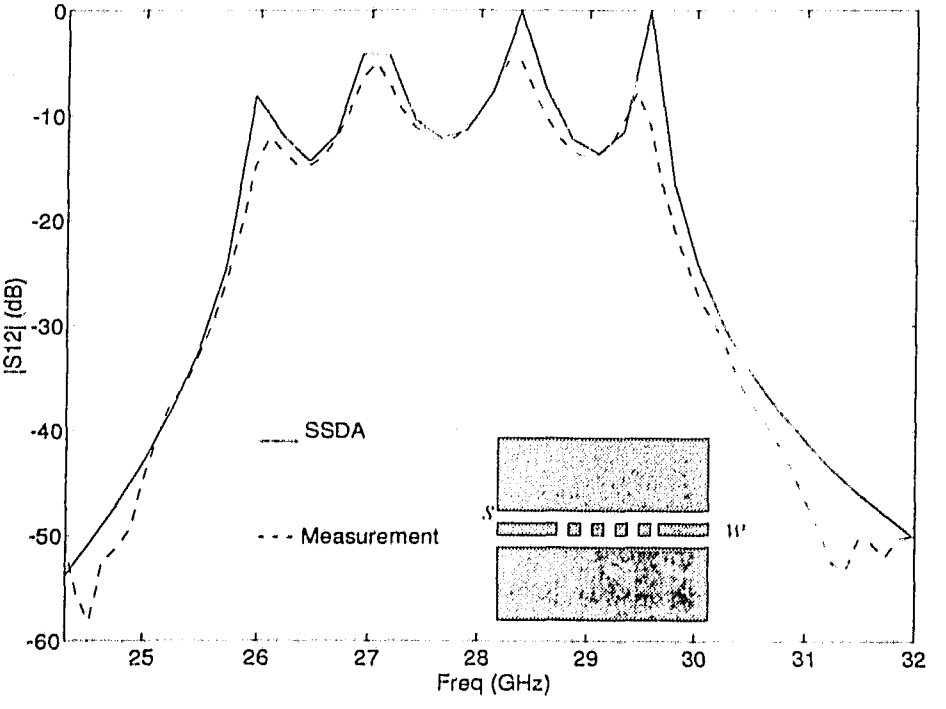

Figure 5.20 S-parameters of a CPW end-coupled filter. *w=0.2, s=0.15, gap width: 25.4μm, resonate length: 2mm.*

Figure 5.20 shows the response of a CPW end-coupled filter. Via holes are also used to short-circuit the ground-plane and the back-metallization. The SSDA simulation exactly predicts the position and magnitude of all four resonant peaks which are generated by this 4-pole filter.

In summary, all experimental results agree with our quasi-static SSDA simulation very well.

Chapter 6

Conclusion

6.1 Contributions

After introducing the generalized form of the Space-Spectral Domain Approach (SSDA), a new deterministic quasi-static SSDA has been developed to analyze planar circuit discontinuities.This new approach extends the SSDA to calculate quasi-static capacitances and S-parameters of arbitrarily shaped planar discontinuities. The discontinuity parameters are derived from an algebraic matrix equation instead of an eigenvalue matrix.

Two new approaches based on the full-wave Space-Spectral Domain Approach (SSDA) have been proposed to calculate scattering parameters for three-dimensional discontinuity problems in MMIC's and MHMIC's. The theory presented in this thesis demonstrates how to implement self-consistent hybrid boundary conditions and how to derive the deterministic approach.

A comparison of the results with other methods and measurements shows excellent agreement up to 40GHz. Results of some complicated structures such as a MHMIC microstrip and CPW taper, CPW air bridge and CPW end-coupled filter are given. Experimental validation of the theoretical results are presented. Although the limited number of examples given is not representative for all type of discontinuities, this technique by nature can treat arbitrary planar two-port circuit contours. This is an advantage of this new method which makes it an attractive CAD tool for engineering applications.

In summary, the major contributions of this dissertation are,

- A generalized SSDA was developed, and a complete field formulation was given.
- A deterministic quasi-static SSDA was introduced.
- The nature of the SSDA was investigated.
- The self consistent hybrid boundary conditions have been developed and implemented into the full-wave SSDA.
- A deterministic full-wave SSDA was developed.
- Experimental work was done to verify the SSDA and to investigate other planar structures.
- A user friendly computer-aided design (CAD) software package, MHMIC 2.0, was developed based on the work of this thesis.

6.2 Future Work

Although extensive simulation and validation were performed in this thesis and a variety of discontinuity modules were included in our CAD software, a user-oriented software can be developed for more complicated discontinuities. Another approach is to use the SSDA algorithm to generate libraries for certain popular CAD packages such as TOUCHSTONE^{TM} or SUPER COMPACT^{TM}.

The quasi-static SSDA is a very efficient tool to analyze most planar circuits. It can be extended to opto-electronic applications, e.g., for the analysis of field distribution of an electro-optical modulator as shown in Figure 6.1.

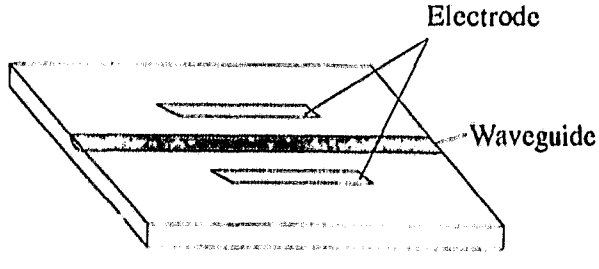

Figure 6.1 Future application: electro-optic modulator

Since the SSDA in its present form does not include the effect of finite metallization thickness and conductor losses, two different approaches are proposed to incorporate finite metallization:

- utilize the concept of surface impedance as it is done in the SDM: add surface impedance into the Green's function to incorporate finite metallization and conductor loss; the formulation will stay mostly the same as in the SSDA.
- using the mode matching method (MMM) in conjunction with the MoL: use MMM in the transverse section to incorporate finite metallization and conductor loss, in the propagation direction (usually called z-direction) the MoL is used as same as in the SSDA.

The SSDA presented in this thesis was applied to a 3-port application in the case of the quasi-static SSDA only (Chapter 5). Its formulation was changed significantly. Without modifying the formulation, both quasi-static and full wave SSDA can be used to analyze in-line multi-port discontinuities as shown in Figure 6.2, because the discretization in the z-direction need not to be changed.

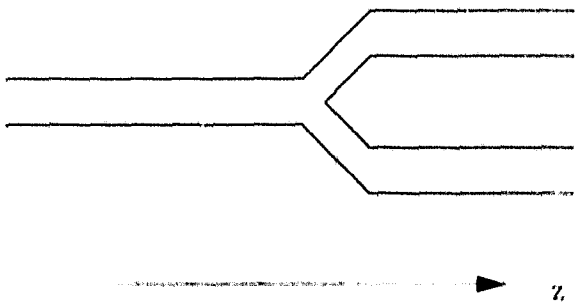

Figure 6.2 An in-line 3-port discontinuity

To analyze arbitrary multi-port discontinuities as shown in Figure 6.3, the z-direction-discretization scheme is not suitable anymore. A possible alternative may be to choose a small region A and develope a discretization scheme that takes into account the

special boundary conditions surrounding region A. Then match the field between the discontinuity region and all connected transmission line separately.

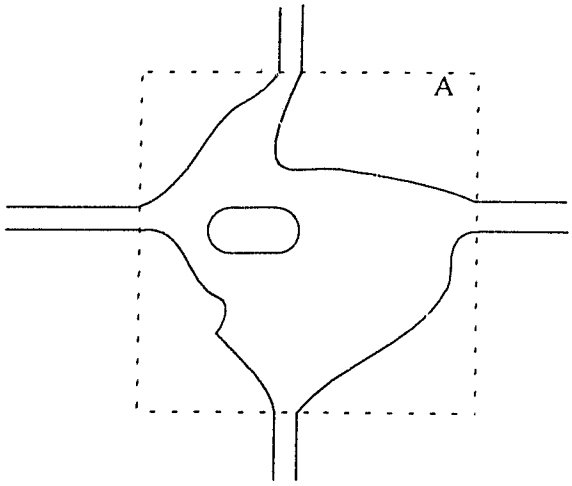

Figure 6.3 Arbitrary multi-port discontinuity

Bibliography

[1] A. Wexler, "Solution of Waveguide discontinuities by modal analysis," *IEEE Trans. on Microwave Theory Tech.*, vol. MTT-15, pp. 508-517, Sept. 1967.

[2] E. Yamashita and R. Mittra, "Variational method for the analysis of microstrip line," *IEEE Trans. on Microwave Theory Tech., vol. MTT*-16, pp. 251-256, Apr. 1968.

[3] R. Mittra and T. Itoh, "A new technique for the analysis of the dispersion characteristics of microstrip lines", *IEEE Trans. on Microwave Theory Tech.*, vol MTT-19, No.1, pp. 47-56, Jan. 1971.

[4] T. Itoh, "Spectral domain immittance approach for dispersion characteristics of generalized printed transmission lines," *IEEE Trans. on Microwave Theory Tech., vol. MTT*-28, pp. 733-736, July 1980.

[5] T. Uwano and T. Itoh, "Spectral domain approach," in *Numerical Techniques for Microwave and Millimeter Wave Passive Structures*, Ch.5, T.Itoh (Ed.), John Wiley, New York, pp. 334-380, 1989.

[6] K.S. Yee, "Numerical solution of initial boundary value problems involving Maxwell's equation", *IEEE Trans. on Antenna and propagation*, Vol. AP-14, pp302-307, May 1966.

[7] O. A.. Liskoverts, "The Method of Lines," *Review, Differ. Uravneniya*, vol.1, pp.1662-1678, 1965.

[8] U. Schulz and R. Pregla, "A new technique for the analysis of the dispersion characteristics of planar waveguide," *Arch. Elek. Ubertragung*, Band 34, pp. 169-173, 1980.

[9] S.B. Worm and R. Pregla, "Hybrid mode analysis of arbitrarily shaped planar microwave structure by the method of lines", *IEEE Trans. on Microwave Theory Tech.*, vol. *MTT*-28, pp.191-196, Feb. 1984.

[10] U. Schultz, "C the edge condition with the method of lines in planar waveguides," *A. E. Elek. Uebertragung.*, vol. 34, pp. 176-178, 1980.

[11] R. Pregla and W. Pascher, "The Method of Lines," in *Numerical Techniques for Microwave and Millimeter Wave Passive Structures*, Ch.5, T.Itoh (Ed.), John Wiley, New York, pp. 381-446, 1989.

[12] S. B. Worm, "Full-wave analysis of discontinuity in planar waveguides by the method of lines using a source approach," *IEEE Trans. on Microwave Theory Tech.*, vol. MTT-38, pp.1510-1514, Oct. 1990.

[13] R. Pregla and W. Pascher, "Diagonalization of difference operators and system matrices in the Method of Lines," *IEEE Microwave and Guided Wave Letters*, Vol. 2, No. 2, pp. 52-54, Feb. 1992.

[14] I. Telliez, A. Couturier, C. Rumelhard, C. Vernaeyen, P. Champion, and D. Fayol, "A compact, monolithic microwave demodulator-modulator for 64QAM digital radio links," *IEEE Trans. on Microwave Theory Tech.*, vol. MTT-39, pp. 1947-1954, Dec. 1991.

[15] H. Diestel and S. B. Worm, "Analysis of hybrid field problems by the method of lines with non-equidistant discretization," *IEEE Trans. on Microwave Theory Tech.*, vol. MTT-32, pp. 633-638, June 1984.

[16] W. J. R. Hoefer, "The transmission line matrix (TLM) method", in *Numerical Techniques for Microwave and Millimeter Wave Passive Structures*, Ch.5, T.Itoh (Ed.), John Wiley, New York, pp. 496-591, 1989.

[17] K. Wu and R. Vahldieck, "A new method of modeling three-dimensional MIC/ MMIC circuits: The space-spectral domain approach," *IEEE Trans. on Microwave Theory and Tech.*, Vol. MTT-32, No.9, pp. 1309-1318, Sept. 1990.

[18] **M. Yu**, K. Wu and R. Vahldieck, "A deterministic quasi-static approach to microstrip discontinuity problem in the space-spectral domain", *IEEE Microwave and Guided Wave Lett.*,Vol. 2, No. 3, pp. 114-116, Mar. 1992.

[19] K. Wu, **M. Yu** and R. Vahldieck, "Rigorous analysis of 3-D planar circuit discontinuities using the space-spectral domain approach (SSDA)," *IEEE Trans. on Microwave Theory and Tech.*, Vol. MTT-40, No. 7, pp. 1475-1483, July 1992.

[20] **M. Yu**, R. Vahldieck and K. Wu, "Theoretical and experimental characterization of coplanar waveguide discontinuities," *IEEE Trans. on Microwave Theory and Tech.*, MTT-41, No.9, Sept., 1993.

[21] J. Martel, R. R. Boix and M. Horno, "Static analysis of microstrip discontinuity using excess charge density in the spectral domain," *IEEE Trans. on Microwave Theory and Tech.*, Vol. MTT-39, No.9, pp. 1623-1631, Sept. 1991.

[22] M. Naghed and I. Wolff, "Equivalent capacitance of coplanar waveguide discontinuities and interdigitated capacitors using a three-dimensional finite difference method", *IEEE Trans. on Microwave Theory and Tech.*, Vol. MTT-38, pp. 1808-1815, Dec. 1990.

[23] W. Veit, H. Diestel and R. Pregla, "Coupling of crossed planar multiconductor systems", *IEEE Trans. on Microwave Theory and Tech.*, MTT-38, no. 3, pp. 265-269, March 1990.

[24] P. Silvester and P. Benedek, "Equivalent capacitance of microstrip open end," *IEEE Trans. on Microwave Theory and Tech.*, MTT-20, pp. 511-516, Aug. 1972.

[25] L. Urshev and A. Stoeva, "Application of equivalent transmission line concept to the method of lines," *Microwave and Optical Technology Letters*, Vol. 3, No. 10, Oct. 1990.

[26] Z. Chen and B. Gao, "Deterministic approach to full-wave analysis of discontinuities in MIC's using the method of lines", *IEEE Trans. on Microwave Theory Tech.*, vol 37, pp.606-611, March 1989.

[27] **M. Yu**, K. Wu and R. Vahldieck, "Analysis of planar circuit discontinuities using the quasi-static space-spectral domain approach," *Proceedings of International Symposium of IEEE Microwave Theory and Tech.*, Albuquerque, USA, June, pp. 545-848, 1992.

[28] H. Yang, N. G. Alexopoulos and D. R. Jackson, "Microstrip open-end and gap discontinuities in a substrate-superstrate structure," *IEEE Trans. on Microwave Theory Tech., MTT-37*, pp. 1542-1546, Oct. 1989.

[29] G. Gronau and I. Wolff, "A simple broad-band device de-embedding method using an automatic network analyzer with time domain option," *IEEE Trans. on Microwave Theory and Tech., MTT-37*, pp. 479-483, Mar. 1989.

[30] N.H.L. Koster, and R. H. Jansen, "The microstrip step discontinuity: a revised description", *IEEE Trans. on Microwave Theory and Tech.*, MTT-34, pp. 213-223, Feb. 1986.

[31] K. Beilenhoff, W. Heinrich, and H.L. Hartnagel, "The scattering behavior of air bridges in coplanar MMIC'S", *Proceedings of the European Microwave Conference* pp. 1131-1135, *1991.*

[32] C. Kuo, T. Kitazawa and T. Itoh, "Analysis of shielded coplanar waveguide step discontinuity considering the finite metallization thickness effect", *Proceedings of 1991 International Symposium of IEEE Microwave Theory and Tech.*, vol.2, pp. 473-475, 1991.

[33] H. Jin and R. Vahldieck, "Calculation of frequency-dependent s-parameters of CPW air-bridge considering finite metallization thickness and conductivity", *Proceedings of 1992 International Symposium of IEEE Microwave Theory and Tech.*, Albuquerque, NM, USA, 1992.

[34] Y. R. Samii, T. Itoh and R. Mittra, "A spectral domain analysis for solving microstrip discontinuities problems," *IEEE Trans. on Microwave Theory Tech.*, MTT-22, pp. 372-378, Apr. 1974.

[35] M. Naghed, M. Rittweger and I. Wolff, "A new method for calculation of the equivalent inductances of coplanar waveguide discontinuities", *Proceedings of 1991 International Symposium of IEEE Microwave Theory and Tech.*, pp. 747-750, 1991.

[36] E. F. Da Silva, M. K. McPhun, "Calibration of an automatic network analyzer system using transmission lines of unknown characteristic impedance, loss and dispersion", *Radio Electron. Eng.*, Vol. 48, No. 5, pp. 227-234, May 1978.

[37] P.R. Shepherd and R. D. Pollard, "Direct calibration and measurement of microstrip structures on gallium arsenide," *IEEE Trans. on Microwave Theory Tech.*, Vol. MTT-34, pp. 1421-1426, No. 1986.

[38] G. R. Engen and C. A. Hoer, "Thru-Reflect-Line: An improved technique for calibrating the dual six-port automatic network analyzer," *IEEE Trans. on Microwave Theory Tech.*, Vol. MTT-27, pp.987-993, Dec. 1979.

[39] R. R. Pantoja, M. J. Howes, J. R. Richardson and R. D. Pollard, "Improved calibration and measurement of the scattering parameters of microwave integrated circuits," *IEEE Trans. on Microwave Theory Tech.*, Vol. MTT-37, pp. 1675-1680, Jan. 1989.

[40] R. Lane, "De-embedding device scattering parameter," *Microwave J.*, Vol.27, pp. 149-156, Aug. 1984.

[41] H. J. Eul and Shiek, "Thru-Match-Reflect: An improved technique for calibrating the dual six-port automatic network analyzer," *Technical Report, Ruhr-University Bochum, Institut fur Hoch and Hochstfrequenztechnik*, Bochum, Germany.

[42] M. Yu, "Microwave Device De-embedding Technique," *Project Report of ELEC454, Microwave and Optical Communication Systems*, Department of Electrical and Computer Engineering, University of Victoria BC, Canada, 1992.

[43] A. Hill and V. K. Tripathi, "An efficient algorithm for the three-dimensional analysis of passive microstrip components and dicontinuities for microwave and millimeter-wave integrated circuits," *IEEE Trans. on Microwave Theory Tech.*, Vol. MTT-39, pp. 83-89, Jan. 1991.

Appendix

The total number of lines in the z-direction:

$$N_z=N_A+N_B,\ N_B=N_{BI}+N_C \tag{E.4}$$

In region A, one unknown is enough to represent C_A^r because of the traveling wave assumption. In region C, the same principle applies. The total number of unknowns:

C_A^r: 1

C_B^{ir}: $N_{BI}+1$

C_A^r and C_B^{ir} can be expressed as

$$C_A^r = c_1\left[1 \quad e^{j\beta h_1} \quad \ldots \quad e^{j\beta h_{N_A}}\right] \tag{E.5}$$

$$C_B^{ir} = \left[a_2, a_3, \ldots, a_{N_{B_1}+1}, a_{N_{B_1}+2}\right]\left[1, e^{j\beta h_{1+N_A+N_B}}, \ldots, e^{j\beta h_{N_{B_1}+N_A+N_B}}\right] \tag{E.6}$$

Combining all left terms of equation (4.27) into one matrix $[W_L]$ yields

$$[W_L]\bar{A} = [W_R]C_A^t \tag{E.7}$$

where

$$[W_R] = \left(\left[W_{11}^t\right]\left[W_{21}^t\right] \quad \left[W_{11}^t\right]\right) \tag{E.8}$$

$\bar{A}=[a_1, a_2, a_3,\ldots,a_{N_{B_1}+2}]$ is the unknown coefficient vector.

When $N_A>N_{BI}+2$, equation (4.27) can be solved.